

On a nonlinear nonlocal reaction-diffusion system applied to image restoration

Yuhang Li ^a, Zhichang Guo ^a, Jingfeng Shao ^{a,b,*}, Boying Wu ^a

^aThe Department of Mathematics, Harbin Institute of Technology, Harbin 150001, China

^bCollege of Mathematics and Information Science, Guangxi University, Nanning 530004, China

Abstract

This paper deals with a novel nonlinear coupled nonlocal reaction-diffusion system proposed for image restoration, characterized by the advantages of preserving low gray level features and textures. The gray level indicator in the proposed model is regularized using a new method based on porous media type equations, which is suitable for recovering noisy blurred images. The well-posedness, regularity, and other properties of the model are investigated, addressing the lack of theoretical analysis in those existing similar types of models. Numerical experiments conducted on texture and satellite images demonstrate the effectiveness of the proposed model in denoising and deblurring tasks.

Keywords: nonlinear nonlocal parabolic equations, fractional derivatives, reaction-diffusion system, maximal regularity, image processing

1. Introduction

1.1. Diffusions and regularizations for image restoration

In many image processing applications, the acquired images are often blurred and corrupted by noise [67, 17]. The degradation model of an image can typically be formulated as $f = Ku^\dagger + n$, where K is some linear operator, especially convolution operator, n is noise, f is the observed image, and u^\dagger is the original image. In this paper, we mainly focus on the non-blind image restoration problem, which aims to recover a clean image u from a noisy blurred image f when K is known exactly. As this is an ill-posed inverse problem, regularization techniques are often required, typically through the minimization of the following energy functional:

$$E(u) = \Phi(u) + \frac{\lambda}{2} \|Ku - f\|_2^2, \quad (1.1)$$

where $\|Ku - f\|_2^2$ is called the fidelity term and $\Phi(u)$ is called the regularization term, $\lambda \geq 0$ is a parameter to balance the fidelity term and regularization term [17, 7]. The regularization term $\Phi(u)$ imposes a priori constraint on the unknown minimizer u and is generally chosen as $\frac{1}{2} \int_{\Omega} G(|\nabla u|^2) dx$ in earlier methods, yielding the gradient flow (or the subgradient flow if E is not Fréchet differentiable) corresponding to (1.1) as

$$u_t = \operatorname{div} (g(|\nabla u|^2) \nabla u) - \lambda K'(Ku - f) \quad (1.2)$$

is a reaction-diffusion equation, where K' is the adjoint operator of K , $G : \mathbb{R}_{\geq 0} \rightarrow \mathbb{R}$, $g(s) = \frac{d}{ds} G(s)$. Many models have been proposed for image restoration. Quadratic Tikhonov regularization [59], which amounts

*Corresponding author.

Email addresses: mathlyh@stu.hit.edu.cn (Yuhang Li ^a), mathgzc@hit.edu.cn (Zhichang Guo ^a), sjfmath@163.com (Jingfeng Shao ^{a,b,*}), mathwby@hit.edu.cn (Boying Wu ^a)

to taking $G(s) = s$ and minimizing (1.1) in $H^1(\Omega)$, leads to the gradient descent flow

$$u_t = \Delta u - \lambda K'(Ku - f), \quad (1.3)$$

and it is well known that sharp edges cannot be preserved under (1.3). In the well-known ROF model proposed by Rudin, Osher and Fatemi [48, 47] (see also [14]), total variation (TV) regularization is employed by selecting $G(s) = 2\sqrt{s}$ and minimizing (1.1) in $BV(\Omega)$, which results in the subgradient flow

$$u_t = \operatorname{div} \left(\frac{\nabla u}{|\nabla u|} \right) - \lambda K'(Ku - f). \quad (1.4)$$

The use of TV can effectively preserve edges but easily cause a staircase effect. Various improved versions [58, 32, 13] have been proposed to eliminate this effect. Another popular class of choices is to employ Perona-Malik diffusion [43, 67], that is, using the flow

$$u_t = \operatorname{div} \left(\frac{1}{1 + k_1 |\nabla u|^2} \nabla u \right) - \lambda K'(Ku - f) \quad (1.5)$$

generated by (1.1) with $G(s) = \frac{1}{k_1} \log(1 + k_1 s)$. Perona-Malik diffusion is a forward-backward diffusion process which is known to sharpen edges effectively but it is mathematically ill-posed and can cause staircase instability [65, 27]. To reduce the noise sensitivity of Perona-Malik diffusion [63], various regularization methods [15, 24, 26, 28] can be utilized to enhance its stability. Higher order regularization terms and PDEs have been proposed to overcome the staircase effect of edge-preserving second-order PDEs. Some early works [72, 38] indicated that methods based on fourth-order PDEs can effectively reduce the staircase effect but encourage piecewise planar solutions, with modification can be found in [11, 29, 68].

Besides being interpreted as a gradient descent flow of an energy functional, a PDE of the form (1.2) can also be directly understood from the perspective of reaction-diffusion equations. From the physical point of view, reaction-diffusion equation describes the evolution of the concentration of a substance in space and time. The diffusion represents the transport of the substance from regions of high concentration to regions of low concentration, and the reaction process accounts for transformation or other dynamic processes [62, 46]. The classical diffusion process for a density function u originates from the principle of mass conservation [40], expressed as

$$u_t + \operatorname{div}(\vec{J}) = 0, \quad (1.6)$$

where \vec{J} denotes the diffusion flux. According to Fick's *first law of diffusion* [40],

$$\vec{J} = -c \nabla u, \quad (1.7)$$

where c is the diffusion coefficient measuring the rate of diffusion. Diffusion has a smoothing effect on spatial heterogeneity, and when the concentration is treated as the gray level at a given location, the diffusion process can be applied to suppress noise in images [64, 9]. If c is a constant, (1.6) reduces to the heat equation, performing isotropic diffusion that smooths the image and thereby eliminates noise. However, it is well-established that smoothing an image using the heat equation is equivalent to convolving it with a Gaussian kernel (indeed, $u(t)$ belongs to the C^∞ class for $t > 0$), which leads to the loss of edge information in the image. In practice, c is usually chosen as a function $c(u)$ depending on u , resulting in *anisotropic* diffusion, so that the diffusion rate varies between certain important image features and other regions in the image, thereby enabling both noise removal and the preservation of these features [9]. By adding the reaction term $-\lambda K'(Ku - f)$ to the right-hand side of (1.6) results in the reaction-diffusion equation

$$u_t = \operatorname{div}(c(u) \nabla u) - \lambda K'(Ku - f), \quad (1.8)$$

which can be applied to image restoration problem introduced at the beginning [67, 41, 76].

In (1.8), the reaction term $-\lambda K'(Ku - f)$ drives u so that Ku approaches f , playing the role of the fidelity term in (1.1), and the diffusion term $\operatorname{div}(c(u)\nabla u)$ smooths u and endows it with some regularity (or makes it belong to certain function spaces), serving a role similar to the regularization term in (1.1). When c is constant, (1.8) corresponds to the gradient descent flow of the Tikhonov regularization (1.3), leading to over-smoothing of the image and blurring of edges and other features. Choosing $c(u) = \frac{1}{|\nabla u|}$ yields (1.4), the subgradient flow of the ROF model, where diffusion is slower in regions with large gradients and faster in regions with small gradients. Such gradient-dependent diffusion coefficients $c(u) = b(|\nabla u|)$, which decrease monotonically with $|\nabla u|$, are also referred to as “edge detectors.” Typical choices include $b(|\nabla u|) = \frac{1}{1+k_1|\nabla u|^2}$ and $b(|\nabla u|) = |\nabla u|^{p-2}$ ($1 < p < 2$), corresponding respectively to Perona-Malik diffusion (1.5) and p -Laplacian-type diffusion. All these choices help slow down diffusion in regions with large gradients, preventing the smoothing effect from destroying edges in the image [9]. The above analysis also shows that, besides choosing different regularization terms in (1.1), one can directly impose a priori information on the solution by designing an appropriate diffusion coefficient. In [77], a doubly degenerate (DD) diffusion model was proposed as a novel image restoration framework, originally utilized for multiplicative noise removal. The framework was described as

$$u_t = \operatorname{div}(c(|\nabla u|, u) \nabla u) - \lambda h(f, u). \quad (1.9)$$

Here $c(|\nabla u|, u) = a(u)b(|\nabla u|)$, where $a(u)$ is chosen to be monotonically increasing in u and is referred to as a gray-level indicator, $b(|\nabla u|)$ is the edge detector described above, and $-\lambda h(u, f)$ represents certain reaction terms derived from variational models. Numerous PDE-based image restoration models can be incorporated into this framework. The gray level indicator is used to control the diffusion rate at different gray levels and the edge detector is employed to preserve image edges; various options are available for selecting both. Typical choices are

$$a(u) = \left(\frac{|u|}{M}\right)^\gamma, \quad b(|\nabla u|) = \frac{1}{1 + k_1|\nabla u|^\beta}, \quad (1.10)$$

where $M = \sup_{x \in \Omega} u(x)$ and $\gamma, k_1, \beta > 0$. With the aid of the gray level indicator and the edge detector, the diffusion rate is reduced in regions with low gray level or large gradients, thereby lessening the smoothing effect that would otherwise destroy faint structures and sharp edges. Taking the reaction term $-\lambda h(f, u)$ in (1.9) to be $-\lambda K'(Ku - f)$, the DD model (1.9) becomes applicable to the restoration of noisy blurred image discussed in this paper.

In summary, reaction-diffusion equations for image restoration can be derived either as the gradient flow of an energy functional or constructed directly by designing an appropriate diffusion coefficient. The latter approach may yield a model that no longer possesses a variational structure like (1.1), but it brings two advantages. Firstly, this approach offers greater flexibility in modeling: by carefully designing the diffusion coefficient one can precisely manipulate the diffusion rate at each pixel, allowing better preservation of desired image features and improved restoration performance. The model also remains interpretable from the reaction-diffusion viewpoint. Secondly, by modifying certain terms in the diffusion coefficient one can turn mathematically ill-posed equations derived from (1.1) into well-posed ones; a typical example is the regularization of the Perona-Malik model (1.5). We will focus mainly on this approach in what follows.

1.2. Nonlocal image restoration models

In natural images, there are often more complex structures such as textures and other repetitive features, which impose higher demands on image restoration models. Nonlocal operators have been defined in [22, 23] to extend the nonlocal method to the variational framework. The nonlocal total variation (NLTV) regularization [23, 75] remains one of the most popular deblurring methods for recovering texture to date. Other image restoration methods based on nonlocal functionals or PDEs [33, 54, 69] have also achieved success in preserving textures. Fractional derivative-based variational and PDE models were proposed in the past two decades for image processing due to the nonlocal property of the fractional derivative. Bai and

Feng [8] proposed a fractional diffusion equation formulated as

$$u_t = \operatorname{div}^\alpha (g(|\nabla^\alpha u|^2) \nabla^\alpha u), \quad (1.11)$$

where $1 < \alpha < 2$, ∇^α denotes the fractional gradient operator and $-\operatorname{div}^\alpha$ denotes the adjoint operator of ∇^α , and the edge detector is chosen as $g(s) = \frac{1}{1+s}$ as in the Perona-Malik model. (1.11) can be regarded as the gradient flow of the energy involving a fractional-order gradient:

$$E(u) = \frac{1}{2} \int_{\Omega} G(|\nabla^\alpha u|^2) dx \quad (1.12)$$

with $g(s) = \frac{d}{ds} G(s)$. This model was proposed for image denoising and can be viewed as generalizations of second-order and fourth-order anisotropic diffusion equations. It has been demonstrated to effectively eliminate the staircase effect. Zhang et al. [74] established a comprehensive total α -order variation framework for image restoration, where α can take any positive value. This framework along with other fractional derivative-based models [16, 71] demonstrates the texture preservation capability in image restoration.

Inspired by the model (1.11) of Bai and Feng, Yao et al. generalized the DD model (1.9) to fractional order, initially applied it for multiplicative noise removal [70], and later extended its application to deblurring tasks [30]. The model takes the form

$$u_t = \operatorname{div}^\alpha (c(|\nabla^\alpha u|, u) \nabla^\alpha u) - \lambda K'(Ku - f), \quad (1.13)$$

where $0 < \alpha < 2$, $c(|\nabla^\alpha u|, u) = a(u)b(|\nabla^\alpha u|)$. The gray level indicator is chosen as

$$a(u) = \left(\frac{|u|}{M} \right)^\gamma, \quad (1.14)$$

where $M = \sup_{x \in \Omega} u(x)$, $\gamma > 0$. On the other hand, $b(|\nabla^\alpha u|) = \frac{1}{1+k_1|\nabla^\alpha u|^\beta}$ can be seen as a texture detection function, where $k_1 > 0$, $\beta > 0$. The design of the diffusion coefficient in this model emphasizes the preservation of low gray level features and texture information. Experimental results have demonstrated the effectiveness of the model in restoring texture-rich images. However, the model (1.13) still faces two challenges: Firstly, since the observed image is always noisy or noisy blurred, the gray level indicator (1.14) may result in a large difference in diffusion rates at neighboring pixels in homogeneous regions, thereby reducing the visual quality of the restored image. Secondly, the model no longer complies with the fundamental diffusion laws (1.6) and (1.7); in particular, the presence of the fractional-order gradient violates mass conservation, which complicates its physical interpretation and increases computational costs. In [53], a model based on (1.6) and fractional Fick's law [51]

$$\vec{J} = -c \nabla^\alpha u \quad (1.15)$$

was proposed for multiplicative noise removal, attempting to address the challenges mentioned above. The model takes on the form

$$u_t = \operatorname{div} (c(|\nabla^\alpha u|, u_\sigma) \nabla^\alpha u), \quad (1.16)$$

where $0 < \alpha \leq 3$, $c(|\nabla^\alpha u|, u_\sigma) = a(u_\sigma)b(|\nabla^\alpha u|)$. The authors chose the gray level indicator as

$$a(u_\sigma) = \left(\frac{|u_\sigma|}{M_\sigma} \right)^\gamma, \quad (1.17)$$

where $u_\sigma = G_\sigma * u$, G_σ is a Gaussian convolution kernel, $M_\sigma = \sup_{x \in \Omega} u_\sigma(x)$, $\sigma, \gamma > 0$. Gaussian filters can reduce the interference of noise on image features, enabling the gray level indicator to perform more effectively in controlling the diffusion rate. Similar operations have also been observed in previous works [39, 52, 78]. The selection of the texture detection function is similar to that in (1.13). This model possesses has a more comprehensive physical background and experimental results have demonstrated that it achieves

superior image restoration performance and fast computational speeds.

1.3. The motivation of the paper

The motivation of this paper is to propose an anisotropic diffusion model from a clear physical background, with the aim of preserving low gray level image features and texture details in denoising and deblurring tasks on both texture-rich images and detailed satellite images. A simple idea is to consider the equation

$$u_t = \operatorname{div} (c(|\nabla^\alpha u|, u_\sigma) \nabla u) - \lambda K'(Ku - f), \quad (1.18)$$

and select the same gray level indicator as in (1.16). However, this is not suitable for restoring noisy blurred images because the Gaussian filter makes the already blurred image *over smooth* (u_σ belongs to the C^∞ class), which would result in a rough gray level indication and decrease the visual quality of the restored image. This requires us to adopt a “gentler” approach to regularize u in (1.14). The gray level indicator in (1.14) was initially inspired by the gamma correction [77, 44], but we now provide another interpretation. In DD model (1.9), the gray level indicator ensures that the diffusion is slow when u is small and fast when u is large, which is the characteristic of porous medium equations (PMEs), also known as Newtonian filtration slow diffusion [61]. In fact, if we set $a(u) = \frac{|u|^\gamma}{M^\gamma}$, $b(\cdot) \equiv 1$, $h(f, u) = 0$ in the DD model (1.9), and taking M as a positive constant, such as $M = \sup_{x \in \Omega} f(x)$, (1.9) becomes a PME:

$$u_t = \frac{M^{-\gamma}}{\gamma + 1} \operatorname{div} (|u|^\gamma \nabla u) = \frac{M^{-\gamma}}{\gamma + 1} \Delta |u|^{\gamma+1}. \quad (1.19)$$

This type of equation appears in different contexts, such as in the flow of gases through porous media [10, 42], in the heat conduction at high temperatures [73] and in groundwater flow [12]. For the case where $b(\cdot)$ is chosen as a general edge detection operator, the equation

$$u_t = \operatorname{div} \left(\frac{|u|^\gamma}{M^\gamma} b(|\nabla u|) \nabla u \right)$$

can be viewed as an *anisotropic* PME.

Inspired by the analysis above, we consider introducing a variable v into the gray value indicator, designing it to satisfy a type of slow diffusion equation and ensuring it has the same initial datum as u , so that it gradually becomes more regular during the diffusion process, rather than always remaining smooth like u_σ in (1.17). The diffusion equation for denoising and deblurring is written as

$$u_t = \operatorname{div} \left(\frac{|v|^\gamma}{M^\gamma} \frac{1}{1 + k_1 |\nabla^\alpha u|^\beta} \nabla u \right) - \lambda K'(Ku - f). \quad (1.20)$$

To emphasize mutual transfer of information between the two equations, we design the diffusion equation for v as

$$v_t = \lambda_1 \operatorname{div} \left(\frac{|u|^\mu}{M^\mu} \nabla v \right) + (1 - \lambda_1) \operatorname{div} \left(\frac{|v|^\gamma}{M^\gamma} \nabla v \right), \quad (1.21)$$

which exhibits characteristics of a PME, where $0 < \lambda_1 < 1$ and $\mu > 0$, the diffusion rate is simultaneously controlled by both u and v . From the viewpoint of PDE evolution, although a rigorous characterization of the asymptotic behavior as $t \rightarrow \infty$ would require further mathematical analysis, it can be qualitatively stated that under the coupled reaction-diffusion system formed by (1.20) and (1.21), u gradually approaches a clearer restored image, while v tends to a smoother function that partially reflects the structural information of u . Specifically, on the right-hand side of (1.21), the slow diffusion term acting on v itself ensures that v becomes smoother over time, while the coupled diffusion term whose coefficient depends on the current image u , locally modulates the diffusion rate of v in a u -weighted manner. Moreover, the regularity of v does not become C^∞ immediately as in the heat equation (for general initial data one typically obtains at most some Hölder regularity [61]). In this way, v receives the desired “gentler” regularization while gradually

absorbing structural information from the gradually clearer u , which in turn provides more reliable gray-level indication for the restoration of u , facilitating positive mutual transfer of information within the system. Besides, following the recommendation in [67], we adopt periodic boundary conditions for this system. Henceforth, for an N -dimensional open cube Ω with side length $L > 0$, we say that a measurable function $u : \Omega \rightarrow \mathbb{R}$ is periodic on Ω if admits an L -periodic extension in each coordinate direction. That is, there exists a measurable function $\tilde{u} : \mathbb{R}^N \rightarrow \mathbb{R}$ such that $\tilde{u}|_{\Omega} = u$ a.e. in Ω and

$$\tilde{u}(x + Le_j) = \tilde{u}(x), \quad \text{for a.e. } x \in \mathbb{R}^N, \quad j = 1, \dots, N,$$

where e_j denotes the j -th standard basis vector of \mathbb{R}^N .

The proposed model. Taking everything into account, we propose the following reaction-diffusion system as an image restoration model for some fixed positive T_0 :

$$\begin{cases} u_t = \operatorname{div}(c(|\nabla^\alpha u|, v) \nabla u) - \lambda K'(Ku - f), & \text{in } (0, T_0) \times \Omega, \\ v_t = \operatorname{div}(a(u, v) \nabla v), & \text{in } (0, T_0) \times \Omega, \\ u, v \text{ periodic on } \Omega & \text{for } (0, T_0), \\ u(0, \cdot) = v(0, \cdot) = f, & \text{in } \Omega, \end{cases} \quad (1.22)$$

where

$$\begin{aligned} c(|\nabla^\alpha u|, v) &= \frac{|v|^\gamma}{M^\gamma} b(|\nabla^\alpha u|), \quad b(|\nabla^\alpha u|) = \frac{1}{1 + k_1 |\nabla^\alpha u|^\beta}, \\ a(u, v) &= \lambda_1 \frac{|u|^\mu}{M^\mu} + (1 - \lambda_1) \frac{|v|^\gamma}{M^\gamma}, \end{aligned}$$

$\Omega \subset \mathbb{R}^N$ is an N -dimensional open cube for $N \geq 1$, $K \in \mathcal{L}(L^1(\Omega), L^2(\Omega))$, $M = \sup_{x \in \Omega} f(x)$, and $0 < \alpha < 1$, $\beta > 0$, $\gamma > 0$, $\mu > 0$, $\lambda > 0$, $0 < \lambda_1 < 1$, $k_1 > 0$ are some given constants. The proposed model maintains the characteristics similar to those of existing models: v can be regarded as a regularized version of the observed image, when v is small, the diffusion at low gray value regions will be slow. The diffusion rate is also controlled by the texture detection function $b(|\nabla^\alpha u|)$, which becomes small when $|\nabla^\alpha u|$ is large, leading to the protection of the textures. Our model also possesses the following advantages: the gentler regularization of u in the gray level indicator aligns the model more closely with the task of recovering noisy blurred images; the model is based on a more classical diffusion framework, providing a *clearer* physical background.

The main contribution of this paper lies in the theoretical analysis of the proposed model. Due to the low regularity of the diffusion coefficient in system (1.22), it is challenging to establish its well-posedness using classical fixed-point methods as done in [39, 52, 78]. Therefore, our work also serves as a *theoretical complement* to equations of the type in [77, 70, 30]. In this paper, we employ Maximal Regularity Theory developed by Amann et al. [3, 4, 5, 34] to investigate the well-posedness of (1.22). The regularity and other properties of solutions are also concerned. Additionally, we present a semi-implicit finite difference scheme for the proposed model and validate its effectiveness in image restoration tasks using both texture and satellite images.

Organization of the paper. The rest of this paper is organized as follows. Some mathematical preliminaries and our main result are stated in Sect. 2. The main result and some properties of weak solutions are proven in Sect. 3. Regularity results for the proposed model are provided in Sect. 4. In Sect. 5, some numerical examples are presented to demonstrate the effectiveness of our model. The concluding remarks are drawn in Sect. 6.

2. Mathematical Preliminaries and main result

In this section, we state some necessary preliminaries of the fractional gradient, fractional order Sobolev spaces and maximal L^p -regularity which will be used below. For simplicity of discussion, throughout the theoretical analysis in this paper, we take Ω to be the normalized unit open cube $(0, 1)^N$. In the following

we will make essential use of two types of periodic Sobolev spaces of fractional order. We refer to [60, 36] as well as [2, Section 5] and the references therein for more basic results of general fractional order Sobolev spaces. Let U be an open set in \mathbb{R}^N and $p \in [1, \infty)$. Denote by

$$[f]_{W^{s,p}(U)} = \left(\int_U \int_U \frac{|f(y) - f(x)|^p}{|x - y|^{N+sp}} dx dy \right)^{\frac{1}{p}}$$

the Gagliardo seminorm of a measurable function f in U for $s \in (0, 1)$. Then for $s \in (0, \infty) \setminus \mathbb{N}$, the periodic Slobodeckij spaces are the Banach spaces defined by

$$W_{\pi}^{s,p}(\Omega) = \left\{ u \in W^{\lfloor s \rfloor, p}(\Omega) : u \text{ is periodic on } \Omega, [D^{\alpha} u]_{W^{s-\lfloor s \rfloor, p}(\Omega)} < \infty, \forall |\alpha| = \lfloor s \rfloor \right\}$$

equipped with the norm

$$\|u\|_{W_{\pi}^{s,p}(\Omega)} = \|u\|_{L_{\pi}^p(\Omega)} + \sum_{|\alpha|=\lfloor s \rfloor} [D^{\alpha} u]_{W^{s-\lfloor s \rfloor, p}(\Omega)},$$

where $\lfloor s \rfloor$ denotes the greatest integer less than or equal to s , and the subscript π indicates that we are in a periodic function space. We will later use Morrey's embedding theorem: for $p \in [1, \infty)$ and $s \in (0, \infty) \setminus \mathbb{N}$ such that $(s - \lfloor s \rfloor)p > N$,

$$W_{\pi}^{s,p}(\Omega) \hookrightarrow C_{\pi}^{\lfloor s \rfloor, s-\lfloor s \rfloor-\frac{N}{p}}(\overline{\Omega}).$$

Readers are referred to [36] for details.

Given $u \in L_{\pi}^1(\Omega)$, its Fourier coefficients are

$$\widehat{u}(k) = \int_{\Omega} u(x) e^{-2\pi i k \cdot x} dx$$

for each $k \in \mathbb{Z}^N$. For $p \in (1, \infty)$ and $s \in (0, \infty)$, we put

$$\|u\|_{H_{\pi}^{s,p}(\Omega)} = \|(I - \Delta)^{\frac{s}{2}} u\|_{L_{\pi}^p(\Omega)},$$

where

$$(I - \Delta)^{\frac{s}{2}} u(x) = \sum_{k \in \mathbb{Z}^N} (1 + 4\pi^2 |k|^2)^{\frac{s}{2}} \widehat{u}(k) e^{2\pi i k \cdot x}.$$

Then the Bessel potential spaces are the Banach spaces defined by

$$H_{\pi}^{s,p}(\Omega) = \{u \in L_{\pi}^p(\Omega) : \|u\|_{H_{\pi}^{s,p}(\Omega)} < \infty\}.$$

It is known from the almost reiteration property [3, Theorem V.1.5.3] that Slobodeckij spaces can be embedded into Bessel potential spaces (see also [60, Theorems 1.3.3(e) and 1.10.3.2]). Specifically, for any $\delta > 0$ and $p \in (1, \infty)$, the embedding

$$W_{\pi}^{s,p}(\Omega) \hookrightarrow H_{\pi}^{s-\delta,p}(\Omega) \tag{2.1}$$

holds for all $s \in (\delta, \infty) \setminus \mathbb{N}$. Furthermore, once $s - \frac{N}{p} \in (0, \infty) \setminus \mathbb{N}$,

$$H_{\pi}^{s,p}(\Omega) \hookrightarrow C_{\pi}^{\kappa, \varrho}(\overline{\Omega}) \tag{2.2}$$

follows from classical embedding theorem [60, Theorems 2.8.1(e) and 4.6.1(e)] and Rychkov's extension theorem [50, Section 5.1.4] (see also [49, Theorem 4.1]), where κ and ϱ denote the integer part and fractional part of $s - \frac{N}{p}$, respectively.

For problem (1.22) to make sense, the fractional gradient ∇^{α} of u needs to be defined. Although certain alternative definitions would work as well, in this paper, we use the frequency domain definition of the

fractional gradient, consistent with those in [8, 24, 29, 71]. For $\alpha \in (0, 1)$, the fractional gradient

$$\nabla^\alpha = (\partial_{x_1}^\alpha, \dots, \partial_{x_N}^\alpha)$$

of u can be represented by the Fourier series

$$\partial_{x_j}^\alpha u(x) = \sum_{k \in \mathbb{Z}^N} (2\pi i k_j)^\alpha \hat{u}(k) e^{2\pi i k \cdot x}.$$

Here, $\partial_{x_j}^\alpha u$ denotes the j -th component of $\nabla^\alpha u$, referred to as the partial derivative with order α of u with respect to x_j , and $(2\pi i k_j)^\alpha = (2\pi |k_j|)^\alpha e^{i\alpha \frac{\pi}{2} \text{sgn}(k_j)}$. The fractional gradient defined in this way is generally not rotation-invariant, in contrast to some other possible definitions such as the Riesz fractional gradient (see [55]). Nevertheless, this definition has the advantage of allowing a straightforward characterization of the mapping properties of fractional derivatives between Bessel potential spaces. Moreover, it is widely employed in image processing because it is easy to implement using fast Fourier transform [8, 24].

We will apply Maximal Regularity Theory to the study of problem (1.22). For more details about this theory, see [3, 4, 5, 34] and the references therein. Let E_0 and E_1 be Banach spaces such that $E_1 \xhookrightarrow{d} E_0$, i.e. E_1 is densely embedded in E_0 . Suppose that $1 < p < \infty$. Set $E_{1-\frac{1}{p}} = (E_1, E_0)_{1-\frac{1}{p}, p}$, $(\cdot, \cdot)_{\theta, p}$ denoting the standard real interpolation functor. Given $T_0 \in (0, \infty)$, for any $T \in (0, T_0]$, put

$$\mathcal{W}^{1,p}(0, T; (E_1, E_0)) = L^p(0, T; E_1) \cap W^{1,p}(0, T; E_0).$$

An operator $A^\sharp \in L^\infty(0, T; \mathcal{L}(E_1, E_0))$ is said to possess the property of maximal L^p -regularity on $[0, T)$ with respect to (E_1, E_0) if the map

$$\mathcal{W}^{1,p}(0, T; (E_1, E_0)) \rightarrow L^p(0, T; E_0) \times E_{1-\frac{1}{p}}, \quad u \mapsto \left(\frac{du}{dt} + A^\sharp u, u(0) \right)$$

is a bounded isomorphism. The set of all such operators A^\sharp is denoted by $\mathcal{MR}^p(0, T; (E_1, E_0))$. Denote by $\mathcal{MR}^p(E_1, E_0)$ the set of all $A^\flat \in \mathcal{L}(E_1, E_0)$ such that the map $[0, T) \rightarrow \mathcal{L}(E_1, E_0), t \mapsto A^\flat$ belongs to $\mathcal{MR}^p(0, T; (E_1, E_0))$. Let X and Y be metric spaces of functions defined on $[0, T)$. A function $f : X \rightarrow Y$ is called a Volterra map (or to possess the Volterra property) if, for each $T \in (0, T_0]$ and each $u, v \in X$ with $u|_{[0, T)} = v|_{[0, T)}$, it follows that $f(u)|_{[0, T)} = f(v)|_{[0, T)}$. Denote by $\mathcal{C}^{0,1}(X, Y)$ the space of all maps $f : X \rightarrow Y$ which are bounded on bounded sets and uniformly Lipschitz continuous on such sets. We write $\mathcal{C}_{\text{Volt}}^{0,1}(X, Y)$ for the subset of all Volterra maps in $\mathcal{C}^{0,1}(X, Y)$. Let Y_1 and Y_0 be Banach spaces of functions defined on $[0, T)$ such that $Y_1 \hookrightarrow Y_0$. Denote by $\mathcal{C}_{\text{Volt}}^{0,1}(X; Y_1, Y_0)$ the set of all Volterra maps $g : X \rightarrow Y_0$ such that $g - g(0) \in \mathcal{C}^{0,1}(X, Y_1)$. Note that the Volterra property is automatic for mappings that are local in time [5]. Indeed, this property is relevant only for problems in which nonlocalities in time are present [25].

Consider a quasilinear abstract Cauchy problem

$$\begin{cases} \frac{du}{dt} + A(u)u = F(u), & t \in (0, T_0), \\ u(0) = u_0. \end{cases} \quad (2.3)$$

A function $u \in \mathcal{W}_{\text{loc}}^{1,p}(0, T; (E_1, E_0))$ is said to be a solution to (2.3) on $[0, T)$ if it satisfies (2.3) in the a.e. sense on $(0, T)$. A solution is said to be maximal if it cannot be extended to a solution on a strictly larger interval.

The following existence and uniqueness result is applied to the study of problem (1.22).

Theorem 2.1. (See [5, Theorem 2.1]) Suppose that

$$(i) \quad A \in \mathcal{C}_{\text{Volt}}^{0,1}(\mathcal{W}^{1,p}(0, T; (E_1, E_0)), \mathcal{MR}^p(0, T; (E_1, E_0)));$$

(ii) there exists $q \in (p, \infty]$ such that

$$F \in \mathcal{C}_{\text{Vot}}^{0,1}(\mathcal{W}^{1,p}(0, T; (E_1, E_0)), L^q(0, T; E_0), L^p(0, T; E_0));$$

(iii) $u_0 \in E_{1-\frac{1}{p}}$.

Then there exist a maximal $T_{\max} \in (0, T_0]$ and a unique solution u of (2.3) on $[0, T_{\max})$.

Henceforth, we always suppose that $0 < T \leq T_0$. Reformulating problem (1.22) as a weak L^p -formulation, the weak solution of (1.22) can be defined as follows.

Definition 2.2. Let $p > 2$. Given $f \in W_{\pi}^{1-\frac{2}{p}, p}(\Omega)$, a couple of functions (u, v) is called a weak solution to problem (1.22) on $[0, T)$, if it satisfies the following conditions:

- (i) $u, v \in L_{\text{loc}}^p(0, T; W_{\pi}^{1,p}(\Omega)) \cap W_{\text{loc}}^{1,p}(0, T; W_{\pi}^{-1,p}(\Omega))$;
- (ii) $u(0, \cdot) = v(0, \cdot) = f$;
- (iii) for any $\varphi, \psi \in W_{\pi}^{1,p'}(\Omega)$, the following integral equalities hold:

$$\begin{aligned} \int_{\Omega} u_t \varphi dx + \int_{\Omega} c(|\nabla^{\alpha} u|, v) \nabla u \cdot \nabla \varphi dx + \lambda \int_{\Omega} (Ku - f) K \varphi dx &= 0, \\ \int_{\Omega} v_t \psi dx + \int_{\Omega} a(u, v) \nabla v \cdot \nabla \psi dx &= 0, \end{aligned} \quad (2.4)$$

for almost all $t \in (0, T)$. Here $\frac{1}{p} + \frac{1}{p'} = 1$.

We will reduce the study of weak solutions to (1.22) to that of solutions to a quasilinear abstract Cauchy problem of the form (2.3). The main result is stated as follows.

Theorem 2.3. Assume that $p \in \left(\frac{2+N}{1-\alpha}, \infty\right)$ and $\beta \geq 1$. Let $f \in W_{\pi}^{1-\frac{2}{p}, p}(\Omega)$ with $f \geq 0$ and bounded away from zero a.e. in Ω . Then there exist a unique maximal $T_{\max} \in (0, T_0]$ and a unique weak solution (u, v) of problem (1.22) on $[0, T_{\max})$.

The proof of Theorem 2.3 is carried out within the framework of Maximal Regularity Theory, incorporating the techniques developed in [24, 25, 29], with details given in the next section.

3. Local well-posedness and some properties of weak solutions

In this section, we first establish the local well-posedness of problem (1.22) via maximum regularity. For all $\varepsilon > 0$, let $\bar{v}_{\varepsilon} = \max\{v, \varepsilon\}$. We consider the following auxiliary problem:

$$\begin{cases} u_t = \text{div}(c(|\nabla^{\alpha} u|, \bar{v}_{\varepsilon}) \nabla u) - \lambda K'(Ku - f), & \text{in } (0, T_0) \times \Omega, \\ v_t = \text{div}(a(u, \bar{v}_{\varepsilon}) \nabla v), & \text{in } (0, T_0) \times \Omega, \\ u, v \text{ periodic on } \Omega, & \text{for } (0, T_0), \\ u(0, \cdot) = v(0, \cdot) = f, & \text{in } \Omega. \end{cases} \quad (3.1)$$

Similar to Definition 2.2, we define the weak solution to the auxiliary problem (3.1).

Definition 3.1. Let $p > 2$. Given $f \in W_{\pi}^{1-\frac{2}{p}, p}(\Omega)$, a couple of functions (u, v) is called a weak solution to auxiliary problem (3.1) on $[0, T)$, if it satisfies the following conditions:

- (i) $u, v \in L_{\text{loc}}^p(0, T; W_{\pi}^{1,p}(\Omega)) \cap W_{\text{loc}}^{1,p}(0, T; W_{\pi}^{-1,p}(\Omega))$;

(ii) $u(0, \cdot) = v(0, \cdot) = f$;

(iii) for any $\varphi, \psi \in W_{\pi}^{1,p'}(\Omega)$, the following integral equalities hold:

$$\int_{\Omega} u_t \varphi dx + \int_{\Omega} c(|\nabla^{\alpha} u|, \bar{v}_{\varepsilon}) \nabla u \cdot \nabla \varphi dx + \lambda \int_{\Omega} (Ku - f) K \varphi dx = 0, \quad (3.2a)$$

$$\int_{\Omega} v_t \psi dx + \int_{\Omega} a(u, \bar{v}_{\varepsilon}) \nabla v \cdot \nabla \psi dx = 0, \quad (3.2b)$$

for almost all $t \in (0, T)$.

Remark 3.2. If (u, v) is a weak solution to (3.1) on $[0, T)$, it then follows that v satisfies the minimum principle

$$v(t, x) \geq \operatorname{ess\,inf}_{x \in \Omega} f(x) =: \gamma_f \quad (3.3)$$

holds for every $t \in (0, T)$ and a.e. $x \in \Omega$, as long as $\gamma_f > -\infty$. (3.3) can be immediately proved by Stampacchia's truncation technique. Namely, one may take $\psi = -(v - \gamma_f)_-$ in (3.2b), where $r_- := \max\{-r, 0\}$ for $s \in \mathbb{R}$. Indeed, for a.e. $t \in (0, T)$, $-(v(t, \cdot) - \gamma_f)_-$ belongs to $W_{\pi}^{1,p}(\Omega) \hookrightarrow W_{\pi}^{1,p'}(\Omega)$ (note that $p > 2$), making $\psi = -(v - \gamma_f)_-$ an admissible test function. The proof is standard and is therefore omitted.

Hereafter, we will abbreviate $\operatorname{ess\,inf}$ (resp., $\operatorname{ess\,sup}$) as \inf (resp., \sup). Let B_X denote the unit ball in the Banach space X , and write $B_X(x, R) := x + RB_X$ for the ball centered at x with radius $R > 0$. We now present the proof of Theorem 2.3.

Proof of Theorem 2.3. Firstly, we reformulate problem (3.1) as a quasilinear abstract Cauchy problem. Since $p \in \left(\frac{2+N}{1-\alpha}, \infty\right) \subset (2+N, \infty)$, it follows from Morrey's embedding theorem together with the assumptions on f that

$$f \in C_{\pi}^{0,1-\frac{2+N}{p}}(\bar{\Omega}) \quad \text{and} \quad \inf_{x \in \Omega} f(x) > 0.$$

In this section, we always choose

$$E_0 = W_{\pi}^{-1,p}(\Omega)^2, \quad E_1 = W_{\pi}^{1,p}(\Omega)^2.$$

For this choice it is well-known that $E_1 \xrightarrow{d} E_0$. We denote by

$$E_{1-\frac{1}{p}} = (E_0, E_1)_{1-\frac{1}{p}, p} = W_{\pi}^{1-\frac{2}{p}, p}(\Omega)^2$$

the respective real interpolation space. To simplify the notation, we set

$$E_0^{1/2} = W_{\pi}^{-1,p}(\Omega), \quad E_1^{1/2} = W_{\pi}^{1,p}(\Omega), \quad E_{1-\frac{1}{p}}^{1/2} = W_{\pi}^{1-\frac{2}{p}, p}(\Omega).$$

For fixed $w_0 = (u_0, v_0)^T \in \mathcal{W}^{1,p}(0, T; (E_1, E_0))$, let a bilinear form $a_{11}[w_0](\cdot, \cdot)$ be given by

$$a_{11}[w_0](u, \varphi) := \int_{\Omega} c(|\nabla^{\alpha} u_0|, \bar{v}_{0\varepsilon}) \nabla u \cdot \nabla \varphi dx, \quad u \in W_{\pi}^{1,p}(\Omega), \varphi \in W_{\pi}^{1,p'}(\Omega).$$

Then a linear differential operator $A_{11}(w_0)$ is naturally induced by $a_{11}[w_0]$, i.e. for almost all $t \in (0, T)$,

$$\langle A_{11}(w_0)u, \varphi \rangle_{(W_{\pi}^{-1,p}(\Omega), W_{\pi}^{1,p'}(\Omega))} = a_{11}[w_0](u, \varphi), \quad \forall \varphi \in W_{\pi}^{1,p'}(\Omega).$$

Actually, we have already defined an operator

$$A_{11} : \mathcal{W}^{1,p}(0, T; (E_1, E_0)) \rightarrow L^{\infty}\left(0, T; \mathcal{L}\left(E_1^{1/2}, E_0^{1/2}\right)\right), \quad w \mapsto A_{11}(w).$$

In the same way, for fixed $w_0 = (u_0, v_0)^T \in \mathcal{W}^{1,p}(0, T; (E_1, E_0))$, let $a_{22}[w_0](\cdot, \cdot)$ be given by

$$a_{22}[w_0](v, \psi) := \int_{\Omega} a(u, \bar{v}_\varepsilon) \nabla v \cdot \nabla \psi dx, \quad v \in W_\pi^{1,p}(\Omega), \psi \in W_\pi^{1,p'}(\Omega),$$

then we can define $A_{22}(w_0)$ by

$$\langle A_{22}(w_0)v, \psi \rangle_{(W_\pi^{-1,p}(\Omega), W_\pi^{1,p'}(\Omega))} = a_{22}[w_0](v, \psi), \quad \forall \psi \in W_\pi^{1,p'}(\Omega)$$

for almost all $t \in (0, T)$, and introduce another operator

$$A_{22} : \mathcal{W}^{1,p}(0, T; (E_1, E_0)) \rightarrow L^\infty(0, T; \mathcal{L}(E_1^{1/2}, E_0^{1/2})), \quad w \mapsto A_{22}(w).$$

Now we define the operator matrix A given by

$$A : \mathcal{W}^{1,p}(0, T; (E_1, E_0)) \rightarrow L^\infty(0, T; \mathcal{L}(E_1, E_0)), \quad w \mapsto \begin{pmatrix} A_{11}(w) & 0 \\ 0 & A_{22}(w) \end{pmatrix}.$$

For fixed $w = (u, v)^T \in \mathcal{W}^{1,p}(0, T; (E_1, E_0))$, we define

$$F : \mathcal{W}^{1,p}(0, T; (E_1, E_0)) \rightarrow L^p(0, T; E_0), \quad w \mapsto \begin{pmatrix} -\lambda K'(Ku - f) \\ 0 \end{pmatrix}. \quad (3.4)$$

Then problem (3.1) can be written as a quasilinear abstract Cauchy problem

$$\begin{cases} \frac{dw}{dt} + A(w)w = F(w), & t \in (0, T_0), \\ w(0) = (f, f)^T, \end{cases} \quad (3.5)$$

Let us now see that the linearized operator matrix has the property of maximal L^p -regularity. It is known that $\partial_{x_j}^\alpha$ has the mapping property between Bessel potential spaces [24, 29], i.e. for any $s \in (\alpha, 1)$,

$$\partial_{x_j}^\alpha \in \mathcal{L}(H_\pi^{s,p}(\Omega), H_\pi^{s-\alpha,p}(\Omega)), \quad j = 1, 2, \dots, N.$$

By combining embeddings (2.1) and (2.2) we know that when $(s - \alpha)p > N$, for any $\delta \in (0, s - \alpha - \frac{N}{p})$,

$$\partial_{x_j}^\alpha \in \mathcal{L}\left(W_\pi^{s,p}(\Omega), C_\pi^{s-\alpha-\frac{N}{p}-\delta}(\bar{\Omega})\right), \quad j = 1, 2, \dots, N. \quad (3.6)$$

Taking $s = 1 - \frac{2}{p}$ in (3.6) and using embedding theorem [3, Theorem III.4.10.2]

$$\mathcal{W}^{1,p}\left(0, T; \left(E_1^{1/2}, E_0^{1/2}\right)\right) \hookrightarrow C\left([0, T], E_{1-\frac{1}{p}}^{1/2}\right) \quad (3.7)$$

we know that for any $u \in \mathcal{W}^{1,p}\left(0, T; \left(E_1^{1/2}, E_0^{1/2}\right)\right)$, there exists $\rho = 1 - \alpha - \frac{N+2}{p} - \delta \in (0, 1)$ such that

$$|\nabla^\alpha u| \in C([0, T], C_\pi^{0,\rho}(\bar{\Omega})).$$

Since $k_1 > 0$ and $\beta \geq 1$, the function $b \in BUC^\infty[0, \infty)$. It follows from the property of Nemytskii operators [18, Theorem 3.1] that

$$g \mapsto b^{(i)}(g), \quad C^{0,\rho_0}(\bar{\Omega}) \rightarrow C^{0,\rho_0}(\bar{\Omega}), \quad i = 0, 1$$

is bounded and uniformly Lipschitz continuous on bounded sets for any $\rho_0 \in (0, 1)$. Therefore,

$$b(|\nabla^\alpha u|) \in C([0, T], C_\pi^{0, \rho}(\bar{\Omega})). \quad (3.8)$$

For any $v \in \mathcal{W}^{1, p}(0, T; (E_1^{1/2}, E_0^{1/2}))$, by (3.7) again we know that

$$\frac{\bar{v}_\varepsilon^\gamma}{M^\gamma} \in C\left([0, T], C_\pi^{0, \gamma(1 - \frac{2+N}{p})}(\bar{\Omega})\right). \quad (3.9)$$

Let $\rho_1 = \min\left\{\rho, \min\{1, \gamma\}\left(1 - \frac{2+N}{p}\right)\right\}$, then $\rho_1 \in (0, 1)$. Combining (3.8) with (3.9), it holds that

$$c(|\nabla^\alpha u|, \bar{v}_\varepsilon) = \frac{\bar{v}_\varepsilon^\gamma}{M^\gamma} b(|\nabla^\alpha u|) \in C([0, T], C_\pi^{0, \rho_1}(\bar{\Omega})) \quad (3.10)$$

since Hölder spaces on $\bar{\Omega}$ are algebras. It follows that

$$[t \mapsto A_{11}(w(t))] \in C\left([0, T], \mathcal{L}\left(E_1^{1/2}, E_0^{1/2}\right)\right) \quad (3.11)$$

for any $w = (u, v)^T \in \mathcal{W}^{1, p}(0, T; (E_1, E_0))$. On the other hand, for each fixed $t \in (0, T)$, the principle symbol of $-A_{11}(w(t)) =: \mathbf{A}_{11}^t$ is

$$\mathcal{A}_{11, \pi}^t(x, \xi) := c(|\nabla^\alpha u(t)|, \bar{v}_\varepsilon(t)) |\xi|^2, \quad x \in \Omega, \quad \xi \in \mathbb{R}^N \setminus \{0\}.$$

From (3.10), it follows that there exists a constant $C_1 > 1$ such that for all $x \in \bar{\Omega}$ and $|\xi| = 1$,

$$0 < \frac{1}{C_1} < \mathcal{A}_{11, \pi}^t(x, \xi) < C_1, \quad (3.12)$$

which implies that $\sigma(\mathcal{A}_{11, \pi}^t) \subset \{\lambda \in \mathbb{C} : \operatorname{Re} \lambda > 0\}$ for all $x \in \bar{\Omega}$ and $|\xi| = 1$. Therefore, for every $t \in (0, T)$, $-A_{11}(w(t))$ is normally elliptic in the sense of Amann [1, 2]. It follows from (3.11) and (3.12) and the weak generation theorem [2, Theorem 8.5] that for every $t \in (0, T)$, $-A_{11}(w(t))$ is sectorial in $E_0^{1/2}$. To obtain the maximal L^p -regularity of $A_{11}(w(t))$, as pointed out in [34, Section 13], the only requirement in the end is sufficient regularity of the coefficients, with Hölder continuity being adequate. Thus, for every $t \in (0, T)$,

$$A_{11}(w(t)) \in \mathcal{MR}^p\left(E_1^{1/2}, E_0^{1/2}\right). \quad (3.13)$$

Similarly, letting $\rho_2 = \min\{\gamma, \mu, 1\}\left(1 - \frac{2+N}{p}\right)$, then we have $\rho_2 \in (0, 1)$. For any $u \in \mathcal{W}^{1, p}(0, T; (E_1^{1/2}, E_0^{1/2}))$, using (3.7) again we deduce that

$$a(u, \bar{v}_\varepsilon) = \lambda_1 \frac{|u|^\mu}{M^\mu} + (1 - \lambda_1) \frac{\bar{v}_\varepsilon^\gamma}{M^\gamma} \in C([0, T], C_\pi^{0, \rho_2}(\bar{\Omega})) \quad (3.14)$$

and that

$$[t \mapsto A_{22}(w(t))] \in C\left([0, T], \mathcal{L}\left(E_1^{1/2}, E_0^{1/2}\right)\right) \quad (3.15)$$

for any $w = (u, v)^T \in \mathcal{W}^{1, p}(0, T; (E_1, E_0))$. For each fixed $t \in (0, T)$, the principle symbol of $-A_{22}(w(t)) =: \mathbf{A}_{22}^t$ is

$$\mathcal{A}_{22, \pi}^t(x, \xi) = a(u(t), \bar{v}_\varepsilon(t)) |\xi|^2, \quad x \in \Omega, \quad \xi \in \mathbb{R}^N \setminus \{0\}.$$

There also exists a constant $C_2 > 1$ such that for all $x \in \bar{\Omega}$ and $|\xi| = 1$,

$$0 < \frac{1}{C_2} < \mathcal{A}_{22, \pi}^t(x, \xi) < C_2, \quad (3.16)$$

which ensures that $-A_{22}(w(t))$ is normally elliptic for every $t \in (0, T)$. Combining (3.14) and (3.16) similarly yields

$$A_{22}(w(t)) \in \mathcal{MR}^p(E_1^{1/2}, E_0^{1/2}) \quad (3.17)$$

for every $t \in (0, T)$. It follows from (3.13) and (3.17) that for all $t \in (0, T)$ and each $G \in L^p(0, T)$, the linear abstract Cauchy problem

$$\begin{cases} \frac{dz}{d\tau} + A(w(t))z = G(\tau), & \tau \in (0, T), \\ z(0) = (0, 0)^T \end{cases}$$

has exactly one strong L^p solution on $(0, T)$, that is

$$A(w(t)) \in \mathcal{MR}^p(E_1, E_0). \quad (3.18)$$

Using [4, Theorem 7.1] in combination with (3.11), (3.15) and (3.18) we obtain that

$$A(w) \in \mathcal{MR}^p(0, T; (E_1, E_0))$$

for any $w \in \mathcal{W}^{1,p}(0, T; (E_1, E_0))$.

Next, we establish Lipschitz estimates of the operator matrix. For $R > 0$, take $w_1 = (u_1, v_1)^T, w_2 = (u_2, v_2)^T \in B_{\mathcal{W}^{1,p}(0, T; (E_1, E_0))}(0, R)$, then

$$\begin{aligned} & \|A(w_1) - A(w_2)\|_{L^\infty(0, T; \mathcal{L}(E_1, E_0))} \\ &= \sup_{t \in [0, T]} \sup_{\substack{w=(u,v)^T \\ \|w\|_{E_1}=1}} \|A(w_1(t))w - A(w_2(t))w\|_{E_0} \\ &= \sup_{t \in [0, T]} \sup_{\|u\|_{E_1^{1/2}}=1} \|A_{11}(w_1(t))u - A_{11}(w_2(t))u\|_{E_0^{1/2}} \\ &\quad + \sup_{t \in [0, T]} \sup_{\|v\|_{E_1^{1/2}}=1} \|A_{22}(w_1(t))v - A_{22}(w_2(t))v\|_{E_0^{1/2}} \\ &= \sup_{t \in [0, T]} \sup_{\substack{\|u\|_{W_\pi^{1,p}(\Omega)}=1, \\ \|\varphi\|_{W_\pi^{1,p'}(\Omega)}=1}} \int_\Omega (c(\overline{v_{1\varepsilon}}(t), |\nabla^\alpha u_1(t)|) - c(\overline{v_{2\varepsilon}}(t), |\nabla^\alpha u_2(t)|)) \nabla u \cdot \nabla \varphi dx \\ &\quad + \sup_{t \in [0, T]} \sup_{\substack{\|v\|_{W_\pi^{1,p}(\Omega)}=1, \\ \|\psi\|_{W_\pi^{1,p'}(\Omega)}=1}} \int_\Omega (a(u_1(t), \overline{v_{1\varepsilon}}(t)) - a(u_2(t), \overline{v_{2\varepsilon}}(t))) \nabla v \cdot \nabla \psi dx \\ &\leq \sup_{t \in [0, T]} M^{-\gamma} \|\overline{v_{1\varepsilon}}(t)^\gamma b(|\nabla^\alpha u_1(t)|) - \overline{v_{2\varepsilon}}(t)^\gamma b(|\nabla^\alpha u_2(t)|)\|_\infty \\ &\quad + \lambda_1 M^{-\mu} \sup_{t \in [0, T]} \| |u_1(t)|^\mu - |u_2(t)|^\mu \|_\infty + (1 - \lambda_1) M^{-\gamma} \sup_{t \in [0, T]} \|\overline{v_{1\varepsilon}}(t)^\gamma - \overline{v_{2\varepsilon}}(t)^\gamma\|_\infty \\ &:= I_1 + I_2 + I_3. \end{aligned}$$

We estimate I_1, I_2 and I_3 separately. From now on $C = C(R)$ denotes a positive constant which can take different value in different places.

$$\begin{aligned} I_1 &\leq C \sup_{t \in [0, T]} \|\overline{v_{1\varepsilon}}(t)^\gamma\|_\infty \|b(|\nabla^\alpha u_1(t)|) - b(|\nabla^\alpha u_2(t)|)\|_\infty \\ &\quad + C \sup_{t \in [0, T]} \|b(|\nabla^\alpha u_2(t)|)\|_\infty \|\overline{v_{1\varepsilon}}(t)^\gamma - \overline{v_{2\varepsilon}}(t)^\gamma\|_\infty \\ &\leq C \sup_{t \in [0, T]} \| |\nabla^\alpha u_1(t)| - |\nabla^\alpha u_2(t)| \|_\infty + C \sup_{t \in [0, T]} \|\overline{v_{1\varepsilon}}(t) - \overline{v_{2\varepsilon}}(t)\|_\infty \end{aligned}$$

$$\begin{aligned}
&\leq C \sup_{t \in [0, T]} \sum_{j=1}^N \left\| \partial_{x_j}^\alpha (u_1(t) - u_2(t)) \right\|_{C_\pi^{0, \rho}(\bar{\Omega})} + C \sup_{t \in [0, T]} \|v_1(t) - v_2(t)\|_{C_\pi^{0, \rho}(\bar{\Omega})} \\
&\leq C \sum_{j=1}^N \left\| \partial_{x_j}^\alpha \right\|_{\mathcal{L}\left(H_\pi^{1-\frac{2}{p}-\delta, p}(\Omega), H_\pi^{1-\alpha-\frac{2}{p}-\delta, p}(\Omega)\right)} \sup_{t \in [0, T]} \|u_1(t) - u_2(t)\|_{W_\pi^{1-\frac{2}{p}, p}(\Omega)} \\
&\quad + C \sup_{t \in [0, T]} \|v_1(t) - v_2(t)\|_{W_\pi^{1-\frac{2}{p}, p}(\Omega)} \\
&\leq C \|u_1 - u_2\|_{C\left([0, T], W_\pi^{1-\frac{2}{p}, p}(\Omega)\right)} + C \|v_1 - v_2\|_{C\left([0, T], W_\pi^{1-\frac{2}{p}, p}(\Omega)\right)}.
\end{aligned}$$

Here we use the fact that $r \mapsto \max\{r, \varepsilon\}$ is a Lipschitz mapping with constant 1. Similarly, we have

$$I_2 \leq C \|u_1 - u_2\|_{C\left([0, T], W_\pi^{1-\frac{2}{p}, p}(\Omega)\right)}, \quad I_3 \leq C \|v_1 - v_2\|_{C\left([0, T], W_\pi^{1-\frac{2}{p}, p}(\Omega)\right)}.$$

Combining the estimates of I_1, I_2 and I_3 , we obtain that

$$\begin{aligned}
&\|A(w_1) - A(w_2)\|_{L^\infty(0, T; \mathcal{L}(E_1, E_0))} \\
&\leq C \left(\|u_1 - u_2\|_{C\left([0, T], E_{1-\frac{1}{p}}^{1/2}\right)} + \|v_1 - v_2\|_{C\left([0, T], E_{1-\frac{1}{p}}^{1/2}\right)} \right) \\
&= C \|w_1 - w_2\|_{C\left([0, T], E_{1-\frac{1}{p}}\right)} \\
&\leq C \|w_1 - w_2\|_{\mathcal{W}^{1, p}(0, T; (E_1, E_0))},
\end{aligned}$$

from which it follows that

$$A \in \mathcal{C}_{\text{Vlt}}^{0, 1}(\mathcal{W}^{1, p}(0, T; (E_1, E_0)), \mathcal{MR}^p(0, T; (E_1, E_0))). \quad (3.19)$$

Now we check the Lipschitz property of the source term. It is clear that $F(0) = (\lambda K' f, 0)^T \in L^\infty(0, T; E_0)$. Set $\tilde{F} = F - F(0) = (-\lambda K' K, 0)^T$. For $R > 0$, take $w_1 = (u_1, v_1)^T, w_2 = (u_2, v_2)^T \in B_{\mathcal{W}^{1, p}(0, T; (E_1, E_0))}(0, R)$, we have that

$$\begin{aligned}
\left\| \tilde{F}(w_1) - \tilde{F}(w_2) \right\|_{L^\infty(0, T; E_0)} &\leq \sup_{t \in [0, T]} \left\| \tilde{F}(w_1(t)) - \tilde{F}(w_2(t)) \right\|_{E_0} \\
&\leq \lambda \sup_{t \in [0, T]} \|K' K (u_1(t) - u_2(t))\|_\infty \\
&\leq C \sup_{t \in [0, T]} \|u_1(t) - u_2(t)\|_{W_\pi^{1-\frac{2}{p}, p}(\Omega)} \\
&\leq C \|w_1 - w_2\|_{C\left([0, T], E_{1-\frac{1}{p}}\right)} \\
&\leq C \|w_1 - w_2\|_{\mathcal{W}^{1, p}(0, T; (E_1, E_0))},
\end{aligned}$$

which implies that

$$F \in \mathcal{C}_{\text{Vlt}}^{0, 1}(\mathcal{W}^{1, p}(0, T; (E_1, E_0)); L^\infty(0, T; E_0), L^p(0, T; E_0)). \quad (3.20)$$

It follows from (3.19), (3.20) and Theorem 2.1 that there exist a maximal $T_{\max} \in (0, T_0]$ and a unique solution $w = (u, v)^T \in \mathcal{W}_{\text{loc}}^{1, p}(0, T_{\max}; (E_1, E_0))$ of the quasilinear abstract Cauchy problem (3.5). Then (u, v) is the unique weak solution to auxiliary problem (3.1) on $[0, T_{\max})$.

Now set $\varepsilon = \inf_{x \in \Omega} f(x)$. Recall the minimum principle mentioned in Remark 3.2 (ii):

$$v(t) \geq \inf_{x \in \Omega} f(x) = \varepsilon \quad \text{a.e. in } \Omega$$

for every $t \in (0, T_{\max})$, which implies that $v = \max\{v, \varepsilon\} = \bar{v}_\varepsilon$. At this point, the concept of a weak solution to problem (3.1) coincides with that of a weak solution to (1.22), which concludes the proof. \square

Remark 3.3. For the well-posedness analysis of (1.22) we require that f be bounded away from zero a.e. in Ω to ensure $\inf_{x \in \Omega} f(x) > 0$. This allows us to rule out the possible degeneracy induced by the factor $|v|^\gamma$ in the diffusion coefficient through the construction of the auxiliary problem (3.1). Introducing such a technical assumption is common in the analysis of image processing models involving gray level indicators; see for example [52, 39]. At the same time, from a modeling viewpoint, a degraded image with additive Gaussian noise may contain negative samples (as Gaussian noise is unbounded), and potential negative values are clamped to 0 before processing. We emphasize that our theoretical development does not cover the case $|\{x \in \Omega : f(x) = 0\}| > 0$; this limitation should not be read as a claim that solutions fail to exist for such initial data; rather, allowing a region of positive measure where f vanishes introduces substantial technical challenges (for instance, loss of normally ellipticity) that are beyond the scope of this paper. Empirically, zero-valued (black) pixels have shown no observable impact on the numerical results reported in Sect. 5. A rigorous theoretical analysis of this more general case is an interesting and challenging open problem left for future work.

A general continuity result [5, Theorem 3.1] for quasilinear parabolic problems implies the continuous dependence of the maximal existence time of solutions on both the initial data and the right-hand side. Utilizing this continuity result, we can derive the following proposition of problem (1.22).

Proposition 3.4. *Let the assumptions of Theorem 2.3 hold. Assume that K satisfies the DC-condition, i.e. $K(1) = 1$, treating $1 \in L^\infty(\Omega)$. Given $\tau \in (0, T_0]$ and $c_* > 0$, there exists $r_0 = r_0(\tau) > 0$ such that for each $f \in B_{W_\pi^{1-\frac{2}{p}, p}(\Omega)}(c_*, r_0)$, the weak solution to problem (1.22) exists on $[0, \tau]$.*

Proof. Note that when f in (1.22) is taken to be the constant $c_* > 0$, the couple $(u, v) \equiv (c_*, c_*)$ is a weak solution to problem (1.22) on $[0, T_0]$. Set $w_0 = (c_*, c_*)^T$, then for any $\tau \in (0, T_0]$, there exists $R > 0$ such that $\|w_0\|_{W^{1,p}(0,\tau;(E_1,E_0))} < R$. It follows from [5, Theorem 3.1] that there exists $r_0 > 0$ such that for any $(f, f)^T \in B_{E_{1-\frac{1}{p}}}(w_0, 2r_0)$, the corresponding maximal interval of existence contains $[0, \tau]$. This fact concludes the proof. \square

For a general K , it is challenging to employ the Stampacchia's truncation method to establish the maximum and minimum principles satisfied by u . However, Theorem 2.3 and Morrey's embedding theorem imply the local solution u is actually bounded. Using the Moser's method, we establish a specific L^∞ estimate for u .

Proposition 3.5. *Let the assumptions of Theorem 2.3 hold. Let (u, v) be the weak solution to problem (1.22) on $[0, T)$ with initial datum f , then for every $t \in (0, T)$,*

$$\|u(t, \cdot)\|_\infty \leq e^{2\lambda t} (\|f\|_\infty + \|K'f\|_\infty). \quad (3.21)$$

Proof. Since $u(t)$ is Hölder continuous, we can take $\varphi = u^{2r-1}(t)$ in (2.4) with $r \geq 1$. Then we have

$$\begin{aligned} \frac{1}{2r} \frac{d}{dt} \int_\Omega u^{2r}(t) dx + (2r-1) \int_\Omega c(|\nabla^\alpha u|, v) u^{2(r-1)} |\nabla u|^2 dx \\ + \lambda \int_\Omega K' K u \cdot u^{2r-1} dx - \lambda \int_\Omega K' f \cdot u^{2r-1} dx = 0. \end{aligned}$$

Applying Young's and Hölder's inequalities, we obtain that

$$\begin{aligned} \frac{1}{2r} \frac{d}{dt} \|u(t, \cdot)\|_{L^{2r}(\Omega)}^{2r} &\leq \frac{\lambda}{2r} \int_{\Omega} |K' K u|^{2r} dx + \frac{2r-1}{2r} \lambda \int_{\Omega} |u|^{2r} dx \\ &\quad + \frac{\lambda}{2r} \int_{\Omega} |K' f|^{2r} dx + \frac{2r-1}{2r} \lambda \int_{\Omega} |u|^{2r} dx \\ &\leq \frac{\lambda}{2r} \|K' f\|_{L^{2r}(\Omega)}^{2r} + \frac{4r-2 + \|K\|^2 |\Omega|}{2r} \lambda \|u(t, \cdot)\|_{L^{2r}(\Omega)}^{2r}. \end{aligned}$$

It follows from Grönwall's inequality that

$$\|u(t, \cdot)\|_{L^{2r}(\Omega)}^{2r} \leq \exp\{(4r-2 + \|K\|^2 |\Omega|) \lambda t\} \left(\|u(0, \cdot)\|_{L^{2r}(\Omega)}^{2r} + \lambda t \|K' f\|_{L^{2r}(\Omega)}^{2r} \right).$$

Using the monotonicity of ℓ^p norms, we arrive the estimate

$$\|u(t, \cdot)\|_{L^{2r}(\Omega)} \leq \exp \left\{ \left(2 + \frac{\|K\|^2 |\Omega| - 2}{2r} \right) \lambda t \right\} \left(\|u(0, \cdot)\|_{L^{2r}(\Omega)} + (\lambda t)^{\frac{1}{2r}} \|K' f\|_{L^{2r}(\Omega)} \right)$$

which yields, as $r \rightarrow \infty$, the estimate (3.21) holds. \square

Now we apply the well-known generalized principle of linearized stability to conclude the following stability result for the equilibria of (1.22). This result pertains to the case of $\lambda = 0$, which leads to a pure diffusion system.

Theorem 3.6. *Let the assumptions of Theorem 2.3 hold. For any given $c_* > 0$, there exists $r_0 > 0$ such that the unique weak solution (u, v) to problem (1.22) with $\lambda = 0$ and initial datum $f \in B_{W_{\pi}^{1-\frac{2}{p}, p}(\Omega)}(c_*, r_0)$ exists globally and converges exponentially in the topology of $W_{\pi}^{1-\frac{2}{p}, p}(\Omega)^2$ to some equilibrium (u_{∞}, v_{∞}) of (1.22) as $t \rightarrow \infty$.*

Proof. It is sufficient to prove that the equilibrium $(c_*, c_*)^T$ is normally stable in $W_{\pi}^{1-\frac{2}{p}, p}(\Omega)^2$ when $\lambda = 0$. For a definition of normally stable, see [45]. Let \mathcal{E} denote the set of equilibrium of (3.5), which means that $w = (u, v)^T \in \mathcal{E}$ if and only if $w \in E_1$ and $A(w)w = 0 = F(w)$, i.e. for any $\varphi, \psi \in W_{\pi}^{1, p}(\Omega)$,

$$\int_{\Omega} c(|\nabla^{\alpha} u|, v) \nabla u \cdot \nabla \varphi dx = \int_{\Omega} a(u, v) \nabla v \cdot \nabla \psi dx = 0. \quad (3.22)$$

It is clear that $\mathcal{E}_0 := \mathbb{R}^2 \subset \mathcal{E}$. At each $w^* = (c_*, c_*)^T \in \mathcal{E}_0$, the linearization of A is given by

$$A_0 := A(w^*) + \frac{d}{dw} [A(w)w^*] \Big|_{w=w^*} = \begin{pmatrix} -c_{11}\Delta & 0 \\ 0 & -c_{22}\Delta \end{pmatrix}$$

where $c_{11} = c_{11}(c_*)$, $c_{22} = c_{22}(c_*) > 0$, $\Delta : W_{\pi}^{1, p}(\Omega) \subset W_{\pi}^{-1, p}(\Omega) \rightarrow W_{\pi}^{-1, p}(\Omega)$. Since the spectrum of $-\Delta$ is discrete and consists only of non-negative eigenvalues, we know that

$$\sigma(A_0) \setminus \{0\} \subset \mathbb{C}_+ = \{z \in \mathbb{C} : \operatorname{Re} z > 0\}$$

and $\{0\}$ is isolated in $\sigma(A_0)$. It follows from $W_{\pi}^{1, p}(\Omega) \hookrightarrow W_{\pi}^{-1, p}(\Omega)$ that A_0 has compact resolvent, which implies that A_0 generates an eventually compact semigroup since $-\Delta$ is sectorial. By [19, Corollary 5.3.2], we can conclude that 0 is a pole of $R(\cdot, A_0)$.

To show 0 is a semi-simple eigenvalue, we will prove that $N(A_0) = N(A_0^2)$. Clearly $N(A_0) = \mathcal{E}_0$, taking $z \in N(A_0^2)$, then there exists $w \in \mathcal{E}_0$ such that $A_0 z = w$. The periodic condition ensures that $w = 0$, and it follows that $z \in N(A_0)$. Therefore, [37, Remark A.2.4] yields that 0 is semi-simple. As \mathcal{E}_0 is a subspace of $W_{\pi}^{1-\frac{2}{p}, p}(\Omega)^2$, the tangent space at w^* is isomorphic to $N(A_0)$.

In [45, Remark 2.2] it is shown that all equilibria close to w^* are contained in a manifold \mathcal{M} of dimension $\dim(N(A_0)) = 2$. Since the dimension of \mathcal{E}_0 is also 2, there exists an open neighborhood $U_0 \subset W_\pi^{1-\frac{2}{p},p}(\Omega)^2$ of w^* such that $\mathcal{M} \cap U_0 = \mathcal{E}_0 \cap U_0$. Thus, U_0 contains no other equilibria than the elements of \mathcal{E}_0 , i.e. $\mathcal{E}_0 \cap U_0 = \mathcal{E} \cap U_0$.

So all assumptions of the generalized principle of linearized stability [45, Theorem 2.1] are satisfied. This principle concludes the proof. \square

Remark 3.7.

- (i) In the general case ($\lambda \neq 0$), the question of whether steady states even exist remains a highly challenging open problem, let alone the analysis of convergence of solutions to such states. In addition, the proposed model (1.22) is not of variational type, making it generally difficult to define a corresponding Lyapunov functional. However, when $\lambda = 0$, it possesses a natural Lyapunov functional given by

$$E = \frac{1}{2} \int_{\Omega} (u^2 + v^2) dx.$$

- (ii) Let the assumptions of Theorem 2.3 hold and (u, v) be the weak solution to problem (1.22) on $[0, T]$ with the initial datum f . If $\lambda = 0$ or $K = I$, the weak solution to problem (1.22) has additionally the following properties:

- (a) (Extremum principle) For every $t \in (0, T)$,

$$\inf_{x \in \Omega} f(x) \leq u(t, x), \quad v(t, x) \leq \sup_{x \in \Omega} f(x), \quad \text{for a.e. } x \in \Omega.$$

- (b) (Average invariance) For every $t \in (0, T)$, it holds that

$$\int_{\Omega} u(t, x) dx = \int_{\Omega} v(t, x) dx = \int_{\Omega} f(x) dx.$$

The proofs are straightforward.

4. Regularity results for the proposed model

In this section, we establish regularity results for the solutions of problem (1.22). Firstly, when the regularity of the initial datum is improved, the local existence and uniqueness of strong solutions to problem (1.22) is obtained via Maximum Regularity Theory. Let $p > 2$. Given $f \in W_\pi^{2-\frac{2}{p},p}(\Omega)$, a couple of functions

$$u, v \in L_{\text{loc}}^p(0, T_{\max}; W_\pi^{2,p}(\Omega)) \cap W_{\text{loc}}^{1,p}(0, T_{\max}; L_\pi^p(\Omega))$$

is called a strong solution to problem (1.22) on $[0, T]$, if it satisfies (1.22) a.e. in $Q_T := (0, T) \times \Omega$.

Theorem 4.1. *Assume that $p \in \left(\frac{2+N}{1-\alpha}, \infty\right)$, $\beta \in \{1\} \cup [2, \infty)$, $\mu > 1$ and $\gamma \geq 1$. Let $f \in W_\pi^{2-\frac{2}{p},p}(\Omega)$ with $f \geq 0$ and bounded away from zero a.e. in Ω . Then there exist a unique maximal $T_{\max} \in (0, T_0]$ such that problem (1.22) possess a unique strong solution (u, v) on $[0, T_{\max})$.*

Proof. The method for proving the local existence and uniqueness of strong solutions is similar to the proof of Theorem 2.3, with the main differences lying in establishing the maximum L^p -regularity of the linearized operator matrix and the Lipschitz estimate between the operator matrix and the source term. Firstly, we

reformulate an auxiliary problem

$$\begin{cases} u_t = c(|\nabla^\alpha u|, \bar{v}_\varepsilon) \Delta u + \nabla c(|\nabla^\alpha u|, v) \cdot \nabla u - \lambda K'(Ku - f), & \text{in } (0, T_0) \times \Omega, \\ v_t = a(u, \bar{v}_\varepsilon) \Delta v + \nabla a(u, v) \cdot \nabla v, & \text{in } (0, T_0) \times \Omega, \\ u, v \text{ periodic on } \Omega & \text{for } (0, T_0), \\ u(0, \cdot) = v(0, \cdot) = f, & \text{in } \Omega, \end{cases} \quad (4.1)$$

as a quasilinear abstract Cauchy problem. In this section, we always choose

$$E_0 = L_\pi^p(\Omega)^2, \quad E_1 = W_\pi^{2,p}(\Omega)^2,$$

which is well-known to satisfy $E_1 \xrightarrow{d} E_0$. Then

$$E_0^{1/2} = L_\pi^p(\Omega), \quad E_1^{1/2} = W_\pi^{2,p}(\Omega), \quad E_{1-\frac{1}{p}} = W_\pi^{2-\frac{2}{p},p}(\Omega)^2, \quad E_{1-\frac{1}{p}}^{1/2} = W_\pi^{2-\frac{2}{p},p}(\Omega).$$

For fixed $w_0 = (u_0, v_0)^T \in \mathcal{W}^{1,p}(0, T; (E_1, E_0))$, we define linear differential operators $A_{11}(w_0)$ and $A_{22}(w_0)$ as follows:

$$\begin{aligned} A_{11}(w_0)u &= -c(|\nabla^\alpha u_0|, \bar{v}_{0\varepsilon}) \Delta u - \nabla c(|\nabla^\alpha u_0|, v_0) \cdot \nabla u, \quad u \in W_\pi^{1,p}(\Omega), \\ A_{22}(w_0)v &= -a(u_0, \bar{v}_{0\varepsilon}) \Delta v - \nabla a(u_0, v_0) \cdot \nabla v, \quad v \in W_\pi^{1,p}(\Omega). \end{aligned}$$

An operator matrix A can then be given by

$$A : \mathcal{W}^{1,p}(0, T; (E_1, E_0)) \rightarrow L^\infty(0, T; \mathcal{L}(E_1, E_0)), \quad w \mapsto \begin{pmatrix} A_{11}(w) & 0 \\ 0 & A_{22}(w) \end{pmatrix}.$$

Defining F as in (3.4), then problem (4.1) can be rewritten as a quasilinear abstract Cauchy problem with the same form as (3.5):

$$\begin{cases} \frac{dw}{dt} + A(w)w = F(w), & t \in (0, T_0), \\ w(0) = (f, f)^T, \end{cases} \quad (4.2)$$

Next, we check the maximal L^p -regularity of the linearized operator matrix. Again, embeddings (2.1) and (2.2) imply that $\delta \in (0, 1 - \alpha - \frac{2+N}{p})$,

$$\partial_{x_j}^\alpha \in \mathcal{L}\left(W_\pi^{2-\frac{2}{p},p}(\Omega), C_\pi^{1,1-\alpha-\frac{N+2}{p}-\delta}(\bar{\Omega})\right), \quad j = 1, 2, \dots, N.$$

It follows from Amann's embedding theorem (3.7) that there exists $\rho = 1 - \alpha - \frac{N+2}{p} - \delta \in (0, 1)$ such that for any $u \in \mathcal{W}^{1,p}\left(0, T; \left(E_1^{1/2}, E_0^{1/2}\right)\right)$,

$$|\nabla^\alpha u| \in C([0, T], C_\pi^{1,\rho}(\bar{\Omega})).$$

The property of Nemytskii operators implies that

$$b(|\nabla^\alpha u|), \quad b'(|\nabla^\alpha u|) \in C([0, T], C_\pi^{0,\rho}(\bar{\Omega})).$$

Set $\rho_0 = 1 - \alpha - \frac{N+2}{p} - \delta$, we choose $\rho_1 = \min\{\rho, \rho_0\}$ if $\gamma = 1$ and $\rho_1 = \min\{\rho, \min\{1, \gamma - 1\}\rho_0\}$ if $\gamma > 1$, then for any $u, v \in \mathcal{W}^{1,p}\left(0, T; \left(E_1^{1/2}, E_0^{1/2}\right)\right)$,

$$c(|\nabla^\alpha u|, \bar{v}_\varepsilon), \quad \partial_{x_j} c(|\nabla^\alpha u|, v) \in C([0, T], C_\pi^{0,\rho_1}(\bar{\Omega})) \quad (4.3)$$

since Hölder spaces on $\overline{\Omega}$ are algebras. It follows that

$$[t \mapsto A_{11}(w(t))] \in C\left([0, T], \mathcal{L}\left(E_1^{1/2}, E_0^{1/2}\right)\right) \quad (4.4)$$

for any $w = (u, v)^T \in \mathcal{W}^{1,p}(0, T; (E_1, E_0))$. On the other hand, as in the proof of Theorem 2.3, for each fixed $t \in (0, T)$ we consider the principal symbol of $\mathbf{A}_{11}^t = -A_{11}(w(t))$, given by

$$\mathcal{A}_{11,\pi}^t(x, \xi) := c(|\nabla^\alpha u(t)|, \bar{v}_\varepsilon(t)) |\xi|^2, \quad x \in \Omega, \quad \xi \in \mathbb{R}^N \setminus \{0\}.$$

It follows from (4.3) that there exists $C_1 > 0$ such that for any $x \in \Omega$ and $|\xi| = 1$,

$$0 < \frac{1}{C_1} < \mathcal{A}_{11,\pi}^t(x, \xi) < C_1,$$

which implies that $\left\{\lambda \in \mathbb{C} : \operatorname{Re} \lambda < \frac{1}{C_1}\right\} \subset \rho(\mathcal{A}_{11,\pi}^t)$ holds for all $x \in \Omega$ and $|\xi| = 1$. $\mathcal{A}_{11,\pi}$ is real, so there exists $\theta \in (0, \frac{\pi}{2})$ such that for all $x \in \Omega$ and $|\xi| = 1$,

$$\sigma(\mathcal{A}_{11,\pi}^t) \subset \left\{\lambda \in \mathbb{C} : \operatorname{Re} \lambda \geq \frac{1}{C_1}\right\} \cap \mathbb{R} \subset \{z \in \mathbb{C} \setminus \{0\} : |\arg(z)| < \theta\}.$$

Thus, $-A_{11}(w(t))$ is uniformly (C_1, θ) -elliptic in the sense of [6, 34] for every $t \in (0, T)$. From [6, Corollary 9.5], it follows that $A_{11}(w(t))$ is a sectorial operator on $L^2(\Omega)$, i.e. $A_{11}(w(t))$ is the generator of an analytic semigroup $T_2(t)$ on $L^2(\Omega)$. [20, Theorem 9.4.2] implies that $T_2(t)$ can be represented by a kernel satisfying a Gaussian bound. It follows from [31, Theorem 3.1] that for any $t \in (0, T)$,

$$A_{11}(w(t)) \in \mathcal{MR}^p\left(E_1^{1/2}, E_0^{1/2}\right). \quad (4.5)$$

Set $\rho_3 = 1 - \frac{N+2}{p}$, we choose $\rho_2 = \min\{1, \mu - 1\}\rho_3$ if $\gamma = 1$ and $\rho_2 = \min\{1, \gamma - 1, \mu - 1\}\rho_3$ if $\gamma > 1$, it is easy to see that for any $u, v \in \mathcal{W}^{1,p}\left(0, T; \left(E_1^{1/2}, E_0^{1/2}\right)\right)$,

$$a(u, \bar{v}_\varepsilon), \quad \partial_{x_j} a(u, v) \in C\left([0, T], C_\pi^{0, \rho_2}(\overline{\Omega})\right),$$

from which it follows that

$$[t \mapsto A_{22}(w(t))] \in C\left([0, T], \mathcal{L}\left(E_1^{1/2}, E_0^{1/2}\right)\right) \quad (4.6)$$

for any $w = (u, v)^T \in \mathcal{W}^{1,p}(0, T; (E_1, E_0))$. The process of obtaining (4.5) reveals that the maximal L^p -regularity of the linearized operator ultimately boils down to sufficient regularity of the coefficients. A similar argument yields that for any $t \in (0, T)$,

$$A_{22}(w(t)) \in \mathcal{MR}^p\left(E_1^{1/2}, E_0^{1/2}\right). \quad (4.7)$$

From (4.5) and (4.7), it follows that for all $t \in (0, T)$ and each $G \in L^p(0, T)$, the linear abstract Cauchy problem

$$\begin{cases} \frac{dz}{d\tau} + A(w(t))z = G(\tau), & \tau \in (0, T), \\ z(0) = (0, 0)^T \end{cases}$$

has a unique strong L^p solution on $(0, T)$, i.e.

$$A(w(t)) \in \mathcal{MR}^p(E_1, E_0). \quad (4.8)$$

By (4.4), (4.6), (4.8) and [4, Theorem 7.1], we can conclude that for any $w \in \mathcal{W}^{1,p}(0, T; (E_1, E_0))$,

$$A(w) \in \mathcal{MR}^p(0, T; (E_1, E_0)).$$

Now we establish Lipschitz estimates of the operator matrix. For $R > 0$, take $w_1 = (u_1, v_1)^T, w_2 = (u_2, v_2)^T \in B_{\mathcal{W}^{1,p}(0, T; (E_1, E_0))}(0, R)$, then

$$\begin{aligned} & \|A(w_1) - A(w_2)\|_{L^\infty(0, T; \mathcal{L}(E_1, E_0))} \\ &= \sup_{t \in [0, T]} \sup_{\substack{w=(u, v)^T \\ \|w\|_{E_1}=1}} \|A(w_1(t))w - A(w_2(t))w\|_{E_0} \\ &= \sup_{t \in [0, T]} \sup_{\|u\|_{E_1^{1/2}}=1} \|A_{11}(w_1(t))u - A_{11}(w_2(t))u\|_{E_0^{1/2}} \\ &\quad + \sup_{t \in [0, T]} \sup_{\|v\|_{E_1^{1/2}}=1} \|A_{22}(w_1(t))v - A_{22}(w_2(t))v\|_{E_0^{1/2}} \\ &:= I_1 + I_2. \end{aligned}$$

We estimate I_1 and I_2 separately. From now on $C = C(R)$ denotes a positive constant which can take different value in different places. Through a process similar to the Lipschitz estimate of A_{11} in the proof of Theorem 2.3, we obtain the following estimate by applying the trick of adding and subtracting the same term repeatedly.

$$\begin{aligned} I_1 &\leq \sup_{t \in [0, T]} \sup_{\|u\|_{W_\pi^{2,p}(\Omega)}=1} \|(c(|\nabla^\alpha u_1|, \bar{v}_{1\varepsilon}) - c(|\nabla^\alpha u_2|, \bar{v}_{2\varepsilon})) \Delta u\|_{L_\pi^p(\Omega)} \\ &\quad + \sup_{t \in [0, T]} \sup_{\|u\|_{W_\pi^{2,p}(\Omega)}=1} \|(\nabla c(|\nabla^\alpha u_1|, v_1) - \nabla c(|\nabla^\alpha u_2|, v_2)) \cdot \nabla u\|_{L_\pi^p(\Omega)} \\ &\leq C \sup_{t \in [0, T]} \|\bar{v}_{1\varepsilon}(t)^\gamma b(|\nabla^\alpha u_1(t)|) - \bar{v}_{2\varepsilon}(t)^\gamma b(|\nabla^\alpha u_2(t)|)\|_\infty \\ &\quad + C \sum_{j=1}^N \sup_{t \in [0, T]} \|v_1(t)^\gamma b(|\nabla^\alpha u_1(t)|)\|_\infty \|\partial_{x_j}(v_1(t) - v_2(t))\|_\infty \\ &\quad + C \sum_{j=1}^N \sup_{t \in [0, T]} \|\partial_{x_j} v_2(t)\|_\infty \|v_1(t)^{\gamma-1} b(|\nabla^\alpha u_1(t)|) - v_2(t)^{\gamma-1} b(|\nabla^\alpha u_2(t)|)\|_\infty \\ &\quad + C \sum_{j=1}^N \sup_{t \in [0, T]} \|v_1(t)^\gamma\|_\infty \|\partial_{x_j}(b(|\nabla^\alpha u_1(t)|) - b(|\nabla^\alpha u_2(t)|))\|_\infty \\ &\quad + C \sum_{j=1}^N \sup_{t \in [0, T]} \|\partial_{x_j} b(|\nabla^\alpha u_2(t)|)\|_\infty \|v_1(t)^\gamma - v_2(t)^\gamma\|_\infty \\ &\leq C \sup_{t \in [0, T]} \|u_1(t) - u_2(t)\|_{W_\pi^{2-\frac{2}{p}, p}(\Omega)} + C \sup_{t \in [0, T]} \|v_1(t) - v_2(t)\|_{W_\pi^{2-\frac{2}{p}, p}(\Omega)} \\ &\quad + C \sum_{j=1}^N \|b'(|\nabla^\alpha u_1(t)|)\|_\infty \|\partial_{x_j}(|\nabla^\alpha u_1(t)| - |\nabla^\alpha u_2(t)|)\|_\infty \\ &\quad + C \sum_{j=1}^N \|\partial_{x_j}(|\nabla^\alpha u_2(t)|)\|_\infty \|b'(|\nabla^\alpha u_1(t)|) - b'(|\nabla^\alpha u_2(t)|)\|_\infty \\ &\leq C \|u_1 - u_2\|_{C([0, T], W_\pi^{2-\frac{2}{p}, p}(\Omega))} + C \|v_1 - v_2\|_{C([0, T], W_\pi^{2-\frac{2}{p}, p}(\Omega))} \end{aligned}$$

$$\begin{aligned}
& + C \sup_{t \in [0, T]} \| |\nabla^\alpha u_1(t)| - |\nabla^\alpha u_2(t)| \|_{C^{1, \rho_1}(\bar{\Omega})} \\
& \leq C \|w_1 - w_2\|_{\mathcal{W}^{1, p}(0, T; (E_1, E_0))}.
\end{aligned}$$

In the same way, we have

$$I_2 \leq C \|w_1 - w_2\|_{\mathcal{W}^{1, p}(0, T; (E_1, E_0))}$$

and furthermore

$$\|A(w_1) - A(w_2)\|_{L^\infty(0, T; \mathcal{L}(E_1, E_0))} \leq C \|w_1 - w_2\|_{\mathcal{W}^{1, p}(0, T; (E_1, E_0))},$$

which implies that

$$A \in \mathcal{C}_{\text{Volt}}^{0,1}(\mathcal{W}^{1, p}(0, T; (E_1, E_0)), \mathcal{MR}^p(0, T; (E_1, E_0))). \quad (4.9)$$

The Lipschitz estimate of the source term is similar to that done in the proof of Theorem 2.3. We have

$$F \in \mathcal{C}_{\text{Volt}}^{0,1}(\mathcal{W}^{1, p}(0, T; (E_1, E_0)); L^\infty(0, T; E_0), L^p(0, T; E_0)). \quad (4.10)$$

It follows from (4.9), (4.10) and Theorem 2.1 that there exist a maximal $T_{\max} \in (0, T_0]$ and a unique solution $w = (u, v)^T \in \mathcal{W}_{\text{loc}}^{1, p}(0, T_{\max}; (E_1, E_0))$ of the quasilinear abstract Cauchy problem (4.2). Now set $\varepsilon = \inf_{x \in \Omega} f(x)$. The minimum principle $v \geq \varepsilon$ implies that $v = \bar{v}_\varepsilon$. At this point, the concept of solution to quasilinear abstract Cauchy problem (4.2) coincides with the concept of strong solution to (1.22). Therefore, (u, v) is the unique strong solution to problem (1.22) on $[0, T_{\max})$, which concludes the proof. \square

Now we present a regularity result for the strong solutions to problem (1.22).

Theorem 4.2. *Let the assumptions of Theorem 4.1 hold. Let (u, v) be the strong solution to problem (1.22) on its maximal interval of existence $[0, T_{\max})$. Then there exists $\rho \in (0, 1)$ such that $u, v \in C^{2+\rho, 1+\frac{\rho}{2}}(\bar{Q}_T)$ for every $T \in (0, T_{\max})$.*

Proof. We will accomplish the proof using the techniques provided in [2, Section 14]. Henceforth, T can take any value in $(0, T_{\max})$, $C > 0$ denotes a constant which can take different value in different places. Theorem 4.1 and Amann's embedding theorem imply that

$$u, v \in L^p(0, T; W_\pi^{2, p}(\Omega)) \cap W^{1, p}(0, T; L_\pi^p(\Omega)) \cap C\left([0, T], W_\pi^{2-\frac{2}{p}, p}(\Omega)\right).$$

Utilizing Hölder's inequality and the interpolation inequality of Slobodeckij spaces, it can be inferred that

$$\begin{aligned}
\|u(t) - u(s)\|_{W_\pi^{(2-\frac{2}{p})\theta, p}(\Omega)} & \leq C \|u(t) - u(s)\|_{L_\pi^p(\Omega)}^{1-\theta} \|u(t) - u(s)\|_{W_\pi^{2-\frac{2}{p}, p}(\Omega)}^\theta \\
& \leq C \left(\int_s^t 1 d\tau \right)^{\frac{1-\theta}{p'}} \left(\int_s^t \|\dot{u}(\tau)\|_{L_\pi^p(\Omega)}^p d\tau \right)^{\frac{1-\theta}{p}} \\
& \leq C |t - s|^{\frac{(1-\theta)(p-1)}{p}}
\end{aligned}$$

holds for all $0 < s \leq t < T$ and $0 < \theta < 1$, from which it follows that

$$u \in C^{\frac{(1-\theta)(p-1)}{p}}\left([0, T], W_\pi^{2\theta-\frac{2\theta}{p}, p}(\Omega)\right).$$

Using arguments similar to those employed in the proofs of Theorems 2.3 and 4.1, it can be deduced that

$$u \in C^{\frac{(1-\theta)(p-1)}{p}}\left([0, T], C_\pi^{1, 2\theta-1-\frac{2\theta+N}{p}}(\bar{\Omega})\right)$$

and

$$|\nabla^\alpha u| \in C^{\frac{(1-\theta)(p-1)}{p}} \left([0, T], C_\pi^{1, 2\theta-1-\frac{2\theta+N}{p}-\alpha-\delta}(\overline{\Omega}) \right)$$

for $\theta \in \left(\frac{N+(\alpha+1)p}{2(p-1)}, 1 \right)$ and $\delta \in \left(0, 2\theta-1-\frac{2\theta+N}{p}-\alpha \right)$. Similarly,

$$v \in C^{\frac{(1-\theta)(p-1)}{p}} \left([0, T], C_\pi^{1, 2\theta-1-\frac{2\theta+N}{p}}(\overline{\Omega}) \right).$$

Set

$$\rho_1 = \frac{(1-\theta)(p-1)}{p}, \quad \rho_2 = 2\theta-1-\frac{2\theta+N}{p}, \quad \rho_3 = 2\theta-1-\frac{2\theta+N}{p}-\alpha-\delta,$$

we choose $\rho = \min\{1, \mu-1\} \min\{\rho_1, \rho_3\}$ if $\gamma = 1$, and $\rho = \min\{1, \gamma-1, \mu-1\} \min_{i=1,2,3} \rho_i$ if $\gamma > 1$, then

$$\partial_{x_j} c(|\nabla^\alpha u|, v), \quad \partial_{x_j} a(u, v), \quad -\lambda K'(Ku - f) \in C^{\rho, \frac{\rho}{2}}(\overline{Q_T})$$

since Hölder spaces on $\overline{\Omega}$ are algebras. Rewrite

$$\begin{aligned} c(|\nabla^\alpha u|, v) &:= a_{11}(t, x), \quad a(u, v) := a_{22}(t, x), \quad -\lambda K'(Ku - f) := f_1(t, x), \\ \nabla c(|\nabla^\alpha u|, v) &:= \mathbf{b}_1(t, x), \quad \nabla a(u, v) := \mathbf{b}_2(t, x), \end{aligned}$$

then u, v turn out to satisfy a.e. in Q_T the following linear parabolic system formulated for \tilde{u} and \tilde{v} :

$$\begin{cases} \tilde{u}_t = a_{11}(t, x)\Delta\tilde{u} + \mathbf{b}_1(t, x) \cdot \nabla\tilde{u} - f_1(t, x), & \text{in } (0, T_0) \times \Omega, \\ \tilde{v}_t = a_{22}(t, x)\Delta\tilde{v} + \mathbf{b}_2(t, x) \cdot \nabla\tilde{v}, & \text{in } (0, T_0) \times \Omega, \\ \tilde{u}, \tilde{v} \text{ periodic on } \Omega & \text{for } (0, T_0), \\ \tilde{u}(0, \cdot) = \tilde{v}(0, \cdot) = f, & \text{on } \Omega, \end{cases} \quad (4.11)$$

since (u, v) is a strong solution to problem (1.22). System (4.11) has Hölder continuous coefficients and a Hölder continuous right-hand side. It follows from classical results [56, Section 14-18] that (4.11) possesses a unique classical solution $u^\bullet, v^\bullet \in C^{2+\rho, 1+\frac{\rho}{2}}(\overline{Q_T})$. Since both (u, v) and (u^\bullet, v^\bullet) satisfy (4.11) in Q_T , we conclude that $u = u^\bullet, v = v^\bullet$. Therefore, $u, v \in C^{2+\rho, 1+\frac{\rho}{2}}(\overline{Q_T})$. \square

Corollary 4.3. *Assume that $\frac{\beta}{2}, \frac{\mu}{2}, \gamma$ are integers, $0 < f \in C_\pi^\infty(\overline{\Omega})$. Let (u, v) be the strong solution to problem (1.22) on its maximal interval of existence $[0, T_{\max})$. Then $u, v \in C^\infty(\overline{Q_T})$ for every $T \in (0, T_{\max})$.*

Proof. The bootstrapping argument used in the proof of Theorem 4.2 can be iterated in order to see that for $k \geq 2$, if $f \in W^{k-\frac{2}{p}, p}(\Omega)$, then there exists $\rho \in (0, 1)$ such that $u, v \in C^{k+\rho, \frac{k+\rho}{2}}(\overline{Q_T})$ by means of classical results [56, Section 14-18], as repeated differentiations can be achieved under the assumption. The arbitrariness of k concludes the proof. \square

5. Numerical experiments

In this section, we present several numerical experiment examples to illustrate the effectiveness of the proposed model in image restoration. Firstly, a numerical discretization of (1.22) is derived. Assume that the discrete image to be $I \times I$ pixels, τ to be the time step size and h the space grid size. Then the equidistant spatio-temporal grid is given by

$$\mathcal{T}_{\tau, h} = \{(t_n, x_i, y_j) : t_n = n\tau, x_i = ih, y_j = jh, n = 0, 1, 2, \dots, i, j = 0, 1, \dots, I-1\}.$$

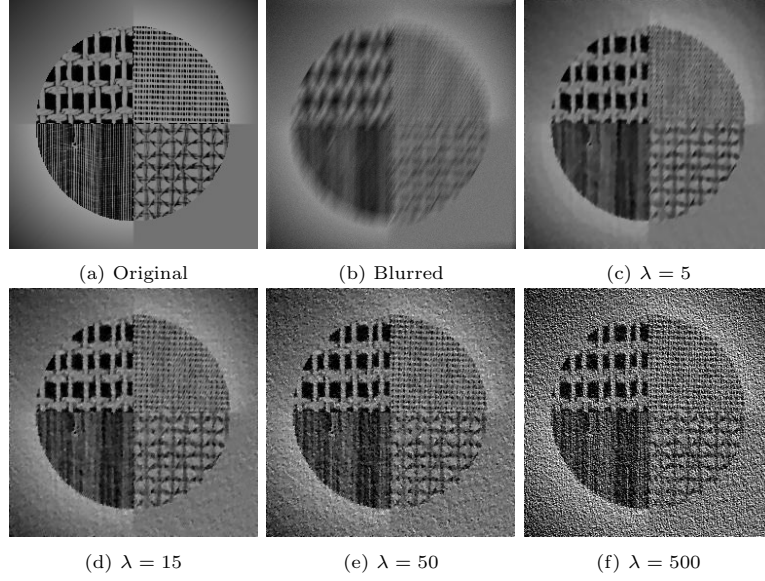


Figure 1: Recovery results of Algorithm 1 on a hybrid image with motion blur and corrupted by the noise of standard deviation $\sigma = 3$ under different λ values. (a) original image. (b) noisy blurred image. (c)-(f) recovered images with $\lambda = 5, 15, 50$ and 500 , respectively.

Denote by $u^n = \{u_{i,j}^n\}_{\forall i,j}$ the grid function at time t_n , which approximates the values of $u(t_n, \cdot)$ at grid points. Some other notations and assumptions are given for the following numerical scheme.

$$\begin{aligned}
u_{i,j}^0 &= f_{i,j} := f(x_i, y_j), \\
u_{i,0}^n &= u_{i,I}^n, \quad u_{0,j}^n = u_{I,j}^n, \quad u_{i,-1}^n = u_{i,I-1}^n, \quad u_{-1,j}^n = u_{I-1,j}^n, \\
D_x^\pm u_{i,j}^n &:= \pm \frac{u_{i\pm 1,j}^n - u_{i,j}^n}{h}, \quad D_y^\pm u_{i,j}^n := \pm \frac{u_{i,j\pm 1}^n - u_{i,j}^n}{h}, \\
\delta_x^2 u_{i,j}^n &:= u_{i+1,j}^n - 2u_{i,j}^n + u_{i-1,j}^n, \quad \delta_y^2 u_{i,j}^n := u_{i,j+1}^n - 2u_{i,j}^n + u_{i,j-1}^n.
\end{aligned}$$

Similar notations and assumptions are used for v and other functions. Denote by \hat{g} the 2-D discrete Fourier transform (DFT) of a grid function g and F^{-1} the 2-D inverse discrete Fourier transform (IDFT) operator. To approximate $|\nabla^\alpha u^n|$, we use a central difference scheme provided by [8]. The fractional-order difference can be defined as

$$\begin{aligned}
D_x^\alpha u^n &= F^{-1} \left[(1 - e^{-i\omega_1 h})^\alpha e^{i\alpha\omega_1 \frac{h}{2}} \hat{u}^n(\omega_1, \omega_2) \right], \\
D_y^\alpha u^n &= F^{-1} \left[(1 - e^{-i\omega_2 h})^\alpha e^{i\alpha\omega_2 \frac{h}{2}} \hat{u}^n(\omega_1, \omega_2) \right],
\end{aligned} \tag{5.1}$$

and the discrete fractional-order gradient $\nabla_h^\alpha u^n = (D_x^\alpha u^n, D_y^\alpha u^n)$. In this section, we focus on the case where K is a convolution operator, namely $Ku = k * u$, where k denotes the convolution kernel. The numerical approximation of (1.22) could be derived by local linearization method. Denote by $a^n = a(u^n, v^n)$ the values at the grid points of the diffusion coefficient $a(\cdot, \cdot)$. If we have a numerical solution (u^n, v^n) , an explicit finite difference scheme

$$\frac{v_{i,j}^{n+1} - v_{i,j}^n}{\tau} = D_x^- (a_{i,j}^n D_x^+ v_{i,j}^n) + D_y^- (a_{i,j}^n D_y^+ v_{i,j}^n), \tag{5.2}$$

can be used to obtain v^{n+1} , then we can use a semi-implicit scheme

$$\begin{aligned}
\frac{u_{i,j}^{n+1} - u_{i,j}^n}{\tau} &= D_x^- (c_{i,j}^n D_x^+ u_{i,j}^n) + D_y^- (c_{i,j}^n D_y^+ u_{i,j}^n) \\
&\quad - \lambda (\mathbf{K}' * \mathbf{K} * u^{n+1})_{i,j} + \lambda (\mathbf{K}' * f)_{i,j},
\end{aligned} \tag{5.3}$$

to obtain u^{n+1} . Here $c^n = c(|\nabla_h^\alpha u^n|, v^{n+1})$, ∇_h^α is the discrete fractional-order gradient, $\mathbf{K} = (k_{i,j})$ is a discrete convolution kernel with adjoint \mathbf{K}' , which is obtained from the convolution kernel k , i.e. $k_{i,j} = k(ih, jh)$. The function f here is only defined on the grid, but we do not denote it.

In the numerical implementation of the proposed model, the explicit scheme (5.2) can be directly computed, and the semi-implicit scheme (5.3) can be solved using the DFT and IDFT. The image restoration process based on the proposed model is summarized as Algorithm 1. The symbol \odot appearing in step 10 denotes element-wise (pointwise) multiplication, i.e. the Hadamard product.

Algorithm 1 The restoration algorithm based on the proposed model

Input: Degraded image f , τ , α , β , k_1 , λ , \mathbf{K} , γ , μ , λ_1 , tol , $maxIter$

Initialize: $u^0 = v^0 = f$, $n = 0$

Output: u^n

```

1: Compute  $M = \max_{i,j} f_{i,j}$ 
2: for each image  $u^n, v^n$  do
3:   Compute  $a^n = \lambda_1 \frac{|u^n|^\mu}{M^\mu} + (1 - \lambda_1) \frac{|v^n|^\gamma}{M^\gamma}$ 
4:   Compute  $v^{n+1}$  by (5.2)
5:   Compute  $D_x^\alpha u^n$  and  $D_y^\alpha u^n$  by (5.1)
6:   Compute  $c^n = \frac{|v^{n+1}|^\gamma}{M^\gamma} \frac{1}{1 + k_1 (D_x^\alpha u^n + D_y^\alpha u^n)^{\beta/2}}$ 
7:   for  $i, j = 0, 1, \dots, I - 1$  do
8:     Compute  $d_{i,j}^n := u_{i,j}^n + \tau (D_x^- (c_{i,j}^n D_x^+ u_{i,j}^n) + D_y^- (c_{i,j}^n D_y^+ u_{i,j}^n)) + \tau \lambda (\mathbf{K}' * f)_{i,j}$ 
9:   end for
10:  Compute  $u^{n+1} = \mathbf{F}^{-1} \left[ \frac{\hat{d}^n}{\hat{I} + \tau \lambda \hat{\mathbf{K}}' \odot \hat{\mathbf{K}}} \right]$ 
11:  if  $\frac{\|u^{n+1} - u^n\|_2}{\|u^{n+1}\|_2} > tol$  and  $i < maxIter$  then
12:    Set  $n = n + 1$ 
13:    Repeat 3-10 steps for  $u^n$  and  $v^n$ 
14:  end if
15: end for

```

In order to quantify the restoration effect, for the original image u^\dagger and the compared image u , the restoration performance is measured in terms of the peak signal noise ratio (PSNR)

$$\text{PSNR}(u, u^\dagger) = 10 \log_{10} \left(\frac{\sum_{i,j} 255^2}{\sum_{i,j} (u_{i,j} - u_{i,j}^\dagger)^2} \right),$$

and the structural similarity index measure (SSIM)

$$\text{SSIM}(u, u^\dagger) = \frac{(2\mu_u \mu_{u^\dagger} + c_1)(2\sigma_{uu^\dagger} + c_2)}{\mu_u^2 + \mu_{u^\dagger}^2 + c_1 + \sigma_u^2 + \sigma_{u^\dagger}^2 + c_2},$$

where c_1, c_2 are two variables to stabilize the division with weak denominator, $\mu_u, \mu_{u^\dagger}, \sigma_u, \sigma_{u^\dagger}$ and σ_{uu^\dagger} are the local means, standard deviations and cross-covariance for image u, u^\dagger , respectively. The better quality image will have higher values of PSNR and SSIM.

	λ	PSNR/SSIM (noisy)	PSNR/SSIM (recovered)
$\sigma = 3$	15	18.07/0.4382	21.17/0.6281
$\sigma = 5$	4.5	18.01/0.3738	20.38/0.6155
$\sigma = 7$	2.5	17.90/0.3091	19.99/0.5905

Table 1: Comparison of the optimal λ values and the corresponding PSNRs/SSIMs at different noise levels σ for the experiments shown in Figs. 1 and 3.

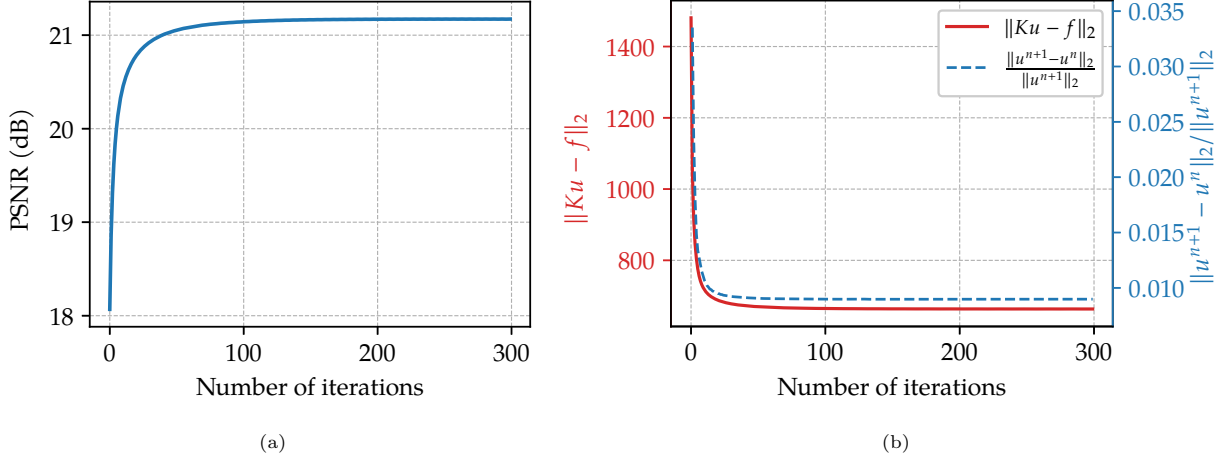


Figure 2: Evolution of PSNR, the data fidelity and the relative error with respect to the iteration number in Algorithm 1, corresponding to the case $\lambda = 15$ in Fig. 1.

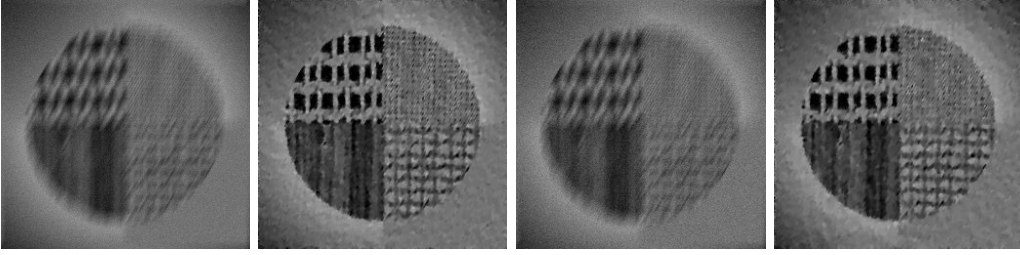


Figure 3: Noisy blurred images and the corresponding restorations by Algorithm 1 with noise levels $\sigma = 5$ (left two columns) and $\sigma = 7$ (right two columns).

We apply Algorithm 1 to a hybrid test image to demonstrate the smoothing effect induced by the diffusion term in the proposed model, as well as the influence of the regularization parameter λ . As shown in Fig. 1b, the test image (originally shown in Fig. 1a) is blurred by a motion blur kernel with an angle of $\frac{\pi}{3}$ and a length of 20, and further distorted by additive isotropic Gaussian noise with a standard deviation of $\sigma = 3$. In this experiment, we set $h = 1$, and use the parameter configuration $\tau = 0.5$, $\alpha = \lambda_1 = 0.9$, $\beta = \gamma = k_1 = 1$ and $\mu = 0.4$ in Algorithm 1, with 300 iterations performed. Figures 1c-1f show the restoration results obtained with different values of λ . It can be observed that when $\lambda = 5$, the image becomes over-smoothed, with the central textured region completely flattened under the smoothing effect of diffusion. When $\lambda = 15$, the algorithm yields the best visual restoration. For $\lambda = 50$, textures appear sharper but the image becomes noticeably noisier, reducing perceived quality. As λ increases to 500, the image is largely buried in noise. Similar behavior is often seen when minimizing the energy (1.1); this is consistent with viewing the diffusion and reaction terms in system (1.22) as playing roles similar to the regularization and fidelity terms in (1.1). In practice, choosing λ appropriately helps balance the contributions of these two terms and can prevent over-smoothing or over-fitting [35]. Figure 2 presents the convergence behavior of Algorithm 1 for the experiment with $\lambda = 15$. As shown in Fig. 2a, PSNR increases rapidly at early iterations and then levels off. Fig. 2b displays the evolution of the data-fidelity residual $\|Ku - f\|_2$ and the relative iteration error $\frac{\|u^{n+1} - u^n\|_2}{\|u^{n+1}\|_2}$, both of which decay quickly at first and subsequently stabilize.

Next, keeping the blur kernel fixed and increasing the added noise to standard deviation $\sigma = 5$ or $\sigma = 7$, we examine how the value of λ required for best visual restoration changes (all other parameters in Algorithm 1 remain the same). Table 1 reports the optimal λ values and the corresponding PSNR and SSIM for $\sigma = 3, 5, 7$. One observes that as the noise level increases, λ needs to be reduced in order to achieve

better visual quality without overfitting; this behavior is similar to the empirical observations [21] made when minimizing the energy (1.1). Figure 3 shows the noisy blurred images for $\sigma = 5$ and $\sigma = 7$ and the corresponding restorations produced by Algorithm 1 using the λ values listed in Table 1.

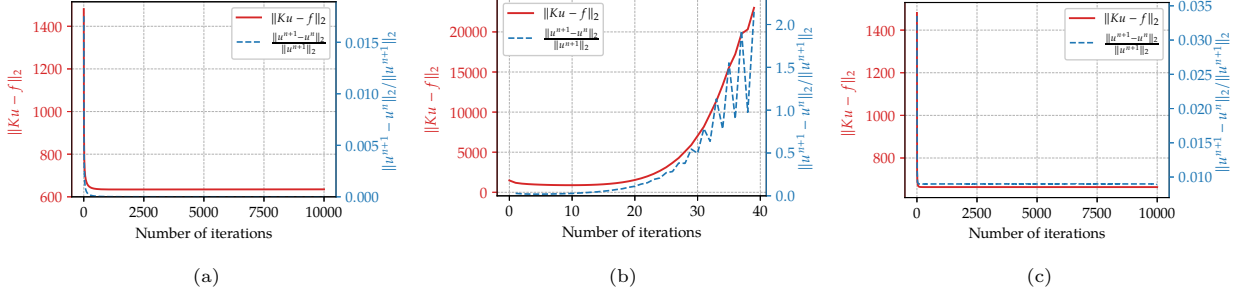


Figure 4: Evolution of the data fidelity and the relative error with respect to the iteration number for the restoration of Fig. 1b using the proposed model with $\lambda = 15$. (a) Explicit scheme (5.8), $\tau = 0.1$, 10 000 iterations. (b) Explicit scheme (5.8), $\tau = 0.15$, 40 iterations. (c) Semi-implicit scheme (5.3), $\tau = 0.5$, 10 000 iterations.

Next we discuss the stability of the numerical scheme for computing u^n . We first consider the stability condition for the semi-implicit scheme (5.3). Freezing $c_{i,j}^n$ as a constant c , consider the following constant coefficient difference equation

$$u_{i,j}^{n+1} = u_{i,j}^n + \frac{\tau c}{h^2} (\delta_x^2 u_{i,j}^n + \delta_y^2 u_{i,j}^n) - \tau \lambda (\mathbf{K}' * \mathbf{K} * u^{n+1})_{i,j}, \quad (5.4)$$

whose stability conditions can be obtained by von Neumann analysis. The term $\lambda(\mathbf{K}' * f)_{i,j}$ in (5.3) is omitted because, by Duhamel's principle, the nonhomogeneous term does not alter the amplification factor (see [57, Section 9.3]). The values of the grid function u^n at each grid point can be represented by its DFT:

$$u_{i,j}^n = \frac{1}{I^2} \sum_{p=0}^{I-1} \sum_{q=0}^{I-1} \hat{u}^n(\omega_1, \omega_2) e^{i(\omega_1 x_i + \omega_2 y_j)}, \quad \omega_1 = \frac{2\pi p}{Ih}, \quad \omega_2 = \frac{2\pi q}{Ih}. \quad (5.5)$$

Noting that the DFT of \mathbf{K}' always equals the complex conjugate of the DFT of \mathbf{K} , utilizing the convolution property of the DFT, we have

$$(\mathbf{K}' * \mathbf{K} * u^{n+1})_{i,j} = \frac{1}{I^2} \sum_{p=0}^{I-1} \sum_{q=0}^{I-1} \hat{u}^{n+1}(\omega_1, \omega_2) |\hat{\mathbf{K}}(\omega_1, \omega_2)|^2 e^{i(\omega_1 x_i + \omega_2 y_j)}. \quad (5.6)$$

Substituting (5.5) and (5.6) into (5.4) and comparing coefficients, we obtain that

$$\begin{aligned} \hat{u}^{n+1}(\omega_1, \omega_2) &= \left[1 - \frac{4\tau c}{h^2} \left(\sin^2 \frac{\omega_1 h}{2} + \sin^2 \frac{\omega_2 h}{2} \right) \right] \hat{u}^n(\omega_1, \omega_2) \\ &\quad - \tau \lambda |\hat{\mathbf{K}}(\omega_1, \omega_2)|^2 \hat{u}^{n+1}(\omega_1, \omega_2). \end{aligned} \quad (5.7)$$

Then the amplification factor can be derived by simple calculation:

$$G(\omega_1, \omega_2) = \frac{\hat{u}^{n+1}(\omega_1, \omega_2)}{\hat{u}^n(\omega_1, \omega_2)} = \frac{1 - \frac{4c\tau}{h^2} \left(\sin^2 \frac{\omega_1 h}{2} + \sin^2 \frac{\omega_2 h}{2} \right)}{1 + \tau \lambda |\hat{\mathbf{K}}(\omega_1, \omega_2)|^2}.$$

The strict stability of the frozen-coefficient scheme (5.4) in the ℓ^2 norm requires the strict von Neumann condition $|G(\omega_1, \omega_2)| \leq 1$ for all ω_1, ω_2 . $G(\omega_1, \omega_2) \leq 1$ holds automatically, whereas ensuring $G(\omega_1, \omega_2) \geq -1$

requires

$$\frac{4\tau c}{h^2} \left(\sin^2 \frac{\omega_1 h}{2} + \sin^2 \frac{\omega_2 h}{2} \right) \leq 2 + \tau \lambda |\hat{\mathbf{K}}(\omega_1, \omega_2)|^2$$

for all ω_1, ω_2 . In particular this must hold at the Nyquist frequency point $(\omega_1^*, \omega_2^*) = (\frac{\pi}{h}, \frac{\pi}{h})$, so we require $\frac{8\tau c}{h^2} \leq 2 + \tau \lambda K_m$, where $K_m := |\hat{\mathbf{K}}(\omega_1^*, \omega_2^*)|^2$. Therefore,

$$\frac{8\tau}{h^2} \max_{n,i,j} c (|\nabla_h^\alpha u^n|, v^{n+1}) \leq 2 + \tau \lambda K_m$$

becomes the necessary condition to ensure that the scheme (5.3) is strictly stable in the ℓ^2 norm.

On the other hand, by a similar procedure one obtains for the explicit scheme

$$\frac{u_{i,j}^{n+1} - u_{i,j}^n}{\tau} = D_x^- (c_{i,j}^n D_x^+ u_{i,j}^n) + D_y^- (c_{i,j}^n D_y^+ u_{i,j}^n) - \lambda (\mathbf{K}' * (\mathbf{K} * u^n - f))_{i,j} \quad (5.8)$$

that the frozen-coefficient scheme has the amplification factor

$$\tilde{G}(\omega_1, \omega_2) = 1 - \frac{4c\tau}{h^2} \left(\sin^2 \frac{\omega_1 h}{2} + \sin^2 \frac{\omega_2 h}{2} \right) - \tau \lambda |\hat{\mathbf{K}}(\omega_1, \omega_2)|^2.$$

Requiring $|\tilde{G}(\omega_1, \omega_2)| \leq 1$ yields

$$\frac{4\tau c}{h^2} \left(\sin^2 \frac{\omega_1 h}{2} + \sin^2 \frac{\omega_2 h}{2} \right) + \tau \lambda |\hat{\mathbf{K}}(\omega_1, \omega_2)|^2 \leq 2$$

for all ω_1, ω_2 . Besides the restriction at the Nyquist frequency point

$$\frac{8\tau}{h^2} \max_{n,i,j} c (|\nabla_h^\alpha u^n|, v^{n+1}) + \tau \lambda K_m \leq 2,$$

strict stability of the explicit scheme in the ℓ^2 norm also requires the constraint at the zero-frequency point $(\omega_1, \omega_2) = (0, 0)$,

$$\tau \lambda |\hat{\mathbf{K}}(0, 0)|^2 \leq 2, \quad (5.9)$$

which imposes stricter restriction on the choice of the time step size. It is well known that $\hat{\mathbf{K}}(0, 0) = \sum_{i,j} k_{i,j}$, and the discrete convolution kernel is usually assumed to satisfy $\sum_{i,j} k_{i,j} = 1$ (see [17, 7]), so (5.9) reduces to $\tau \leq \frac{2}{\lambda}$. For example, when restoring Fig. 1b with $\lambda = 15$, choosing $\tau = 0.1$ and using the explicit scheme (5.8) yields stable behavior after 10 000 iterations, as shown in Fig. 4a, and produces a visually convincing restoration (see Fig. 5a). However, when τ is increased to $0.15 > \frac{2}{\lambda} = \frac{2}{15} \approx 0.133$, the iteration becomes clearly unstable shortly after it starts, as in Fig. 5b, and the restoration is rendered meaningless (see Fig. 4b). By contrast, using the semi-implicit scheme (5.3) with $\tau = 0.5$, the iteration remains stable after 10 000 iterations (Fig. 4a) and yields a good visual restoration result (Fig. 5c).

In deblurring tasks, for relatively small noise levels σ one typically chooses a larger λ to improve restoration fidelity; for example, when $\sigma = 3$ we empirically found that λ on the order of 10^1 gives the best visual results (see the experiments later). When the explicit scheme is employed, the time step τ is constrained by the condition $\tau \leq \frac{2}{\lambda}$; for practical choices of λ , this yields an upper bound on τ that lies roughly between 0.02 and 0.2, resulting in a considerable number of time steps for the deblurring process. The semi-implicit scheme, by contrast, does not incur this additional restriction. To mitigate computational cost, we therefore adopt the semi-implicit scheme (5.3) in the following experiments.

Remark 5.1.

- (i) The strict stability in the ℓ^2 norm demands that $\|u^{n+1}\|_2 \leq \|u^0\|_2 = \|f\|_2$. Since u generally does not satisfy a maximum principle, this condition is somewhat stringent. One may be interested in

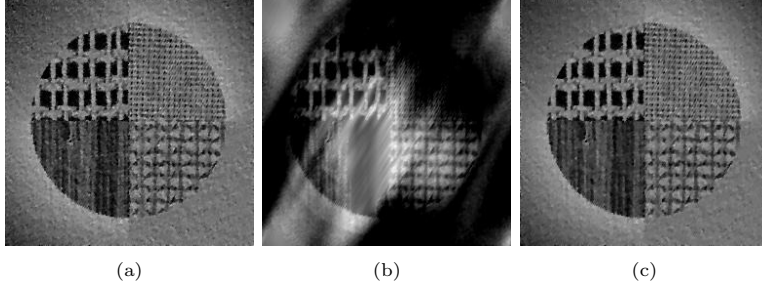


Figure 5: Recovery results of Fig. 1b using the proposed model with $\lambda = 15$. (a) Explicit scheme (5.8), $\tau = 0.1$, 10 000 iterations. (b) Explicit scheme (5.8), $\tau = 0.15$, 40 iterations. (c) Semi-implicit scheme (5.3), $\tau = 0.5$, 10 000 iterations.

employing the generalized von Neumann condition $|G(\omega_1, \omega_2)| \leq 1 + O(\tau)$ to analyze the explicit and semi-implicit schemes in order to obtain sharper stability conditions, but this becomes more involved and requires further investigation. Moreover, as shown in Fig. 4b and Fig. 5b, at the very least, the growth induced by explicitly treating the reaction term is unacceptable.

- (ii) The conditionally stable semi-implicit scheme (5.3) is sufficient for the numerical experiments presented in this paper. However, for images of higher resolution, using larger time steps to reduce computational cost becomes appealing. One possible improvement is to treat the diffusion term implicitly, which leads to the following scheme:

$$\frac{u_{i,j}^{n+1} - u_{i,j}^n}{\tau} = D_x^- (c_{i,j}^n D_x^+ u_{i,j}^{n+1}) + D_y^- (c_{i,j}^n D_y^+ u_{i,j}^{n+1}) - \lambda (\mathbf{K}' * \mathbf{K} * u^{n+1})_{i,j} + \lambda (\mathbf{K}' * f)_{i,j}, \quad (5.10)$$

Because of the variable coefficients, this scheme can no longer be efficiently solved using the DFT. Some operator-splitting methods may be required, and the presence of an implicitly treated reaction term makes the corresponding algorithmic design calls for more in-depth study. In addition, acceleration techniques such as Fast Explicit Diffusion [66] could also be explored to speed up computations based on (5.3), which would be an interesting topic for future work.

We proceed to conduct a series of comparative experiments in which three common types of blur kernels are considered: the motion blur kernel with angle $\frac{\pi}{3}$ and length 20, disk kernel with a radius of 3 and 5×5 average kernel. We test several noisy blurred images, distorted by additive isotropic Gaussian noise with a standard deviation $\sigma = 3$ and by blurring with one of the previously mentioned kernels, to verify the effectiveness of the proposed model. For illustration, the result for the texture1 (256×256 pixels), texture2 (256×256 pixels), hybrid (256×256 pixels), satellite1 (512×512 pixels), satellite2 (512×512 pixels) and satellite3 (512×512 pixels) are presented, see the original test images in Fig. 6.

The proposed model is compared with fast total variation (FastTV) minimization [32], nonlocal total variation (NLTV) method [23, 75], nonlocal adaptive biharmonic (NLABH) regularization [69], a nonlinear fractional diffusion (NFD) model [30] and a Perona-Malik type equation regularized by the p -Laplacian (PLRPM) [28]. The free parameters for FastTV, NLTV, NLABH, NFD and PLRPM are set as suggested in the reference papers. For the proposed model, while there may be more suitable parameter choices for each image, in the following experiments, we set $\tau = 0.5$, $\alpha = 0.9$, $\gamma = 1$, $\mu = 0.4$, $k_1 = 1$, $\lambda_1 = 0.9$, $\max Iter = 500$, and $tol = 0.005$ throughout all experiments. For the texture1, texture2, hybrid, satellite 1, satellite 2 and satellite 3 images, we select $\beta = 0.96, 0.63, 1, 0.7, 0.9$ and 0.8 respectively. The parameter λ is chosen based on the specific image and the type of blur kernel. For a comparison of the performance quantitatively, we list the PSNR and SSIM values of the restored results in Table 2 and Table 3.

Now we report the numerical experiments of deblurring and denoising for the original test images in Fig. 6. The corresponding results are shown in Figs. 7-12. Firstly, the restoration results for texture1

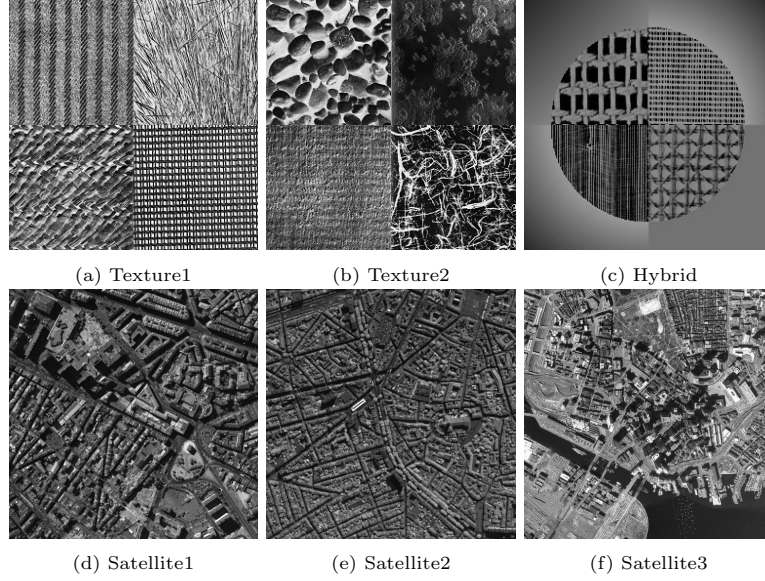


Figure 6: Test images.

Table 2: Comparison of PSNR and SSIM for different models in the experiments on texture1, texture2 and hybrid image. Bold values indicate the best result.

	Figure 7		Figure 8		Figure 9	
	PSNR	SSIM	PSNR	SSIM	PSNR	SSIM
Degraded	12.77	0.1901	15.60	0.3640	18.07	0.4382
FastTV	15.17	0.5320	19.00	0.6887	21.00	0.7136
NLTV	16.35	0.6599	19.26	0.7427	21.14	0.7087
NLABH	16.11	0.6698	18.89	0.6710	20.21	0.4598
NFD	16.18	0.6738	19.06	0.6763	20.36	0.4723
PLRPM	16.30	0.6599	19.29	0.7068	21.17	0.6415
Ours	16.25	0.6745	19.39	0.6992	21.17	0.6281

Table 3: Comparison of PSNR and SSIM for different models in the experiments on three satellite images. Bold values indicate the best result.

	Figure 10		Figure 11		Figure 12	
	PSNR	SSIM	PSNR	SSIM	PSNR	SSIM
Degraded	18.64	0.5171	21.68	0.7761	19.20	0.7680
FastTV	23.97	0.8888	24.91	0.9322	22.41	0.9229
NLTV	23.87	0.8838	25.46	0.9387	22.59	0.9291
NLABH	22.56	0.8475	24.82	0.9325	22.00	0.9049
NFD	22.67	0.8548	24.77	0.9301	22.06	0.9059
PLRPM	24.04	0.8949	25.28	0.9380	22.55	0.9205
Ours	24.44	0.9029	25.47	0.9395	22.55	0.9212

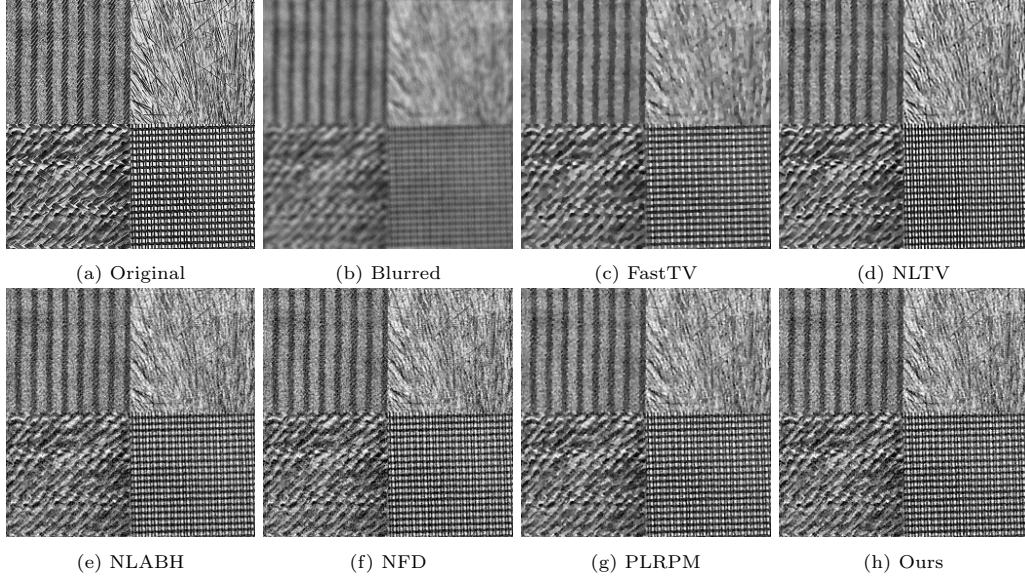


Figure 7: Recovery results for the texture1 image with disk blur and corrupted by the noise of standard deviation $\sigma = 3$. (a) original image. (b) noisy blurred image, PSNR=12.77. (c)-(h) recovered images.

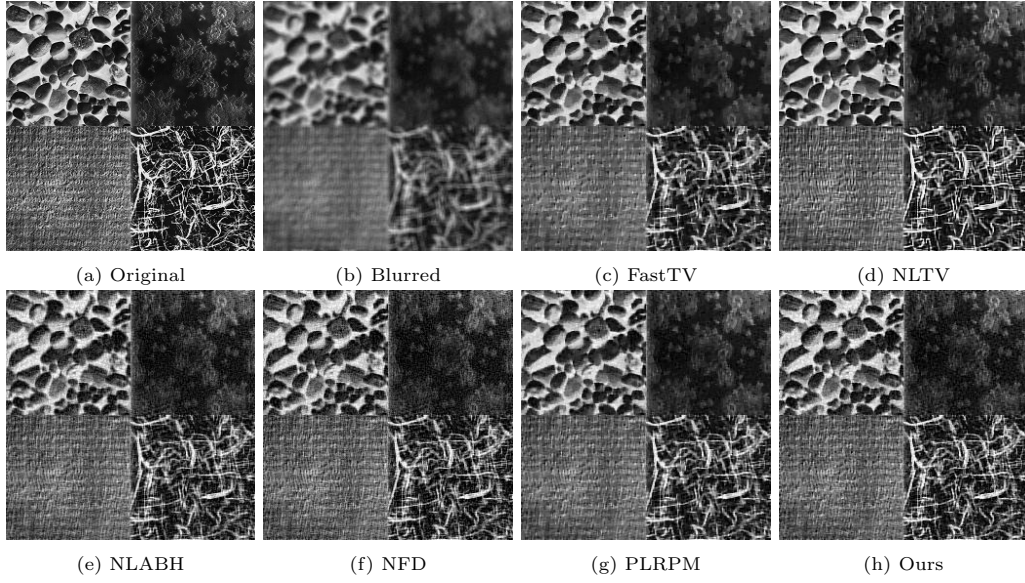


Figure 8: Recovery results for the texture2 image with average blur and corrupted by the noise of standard deviation $\sigma = 3$. (a) original image. (b) noisy blurred image, PSNR=15.60. (c)-(h) recovered images.

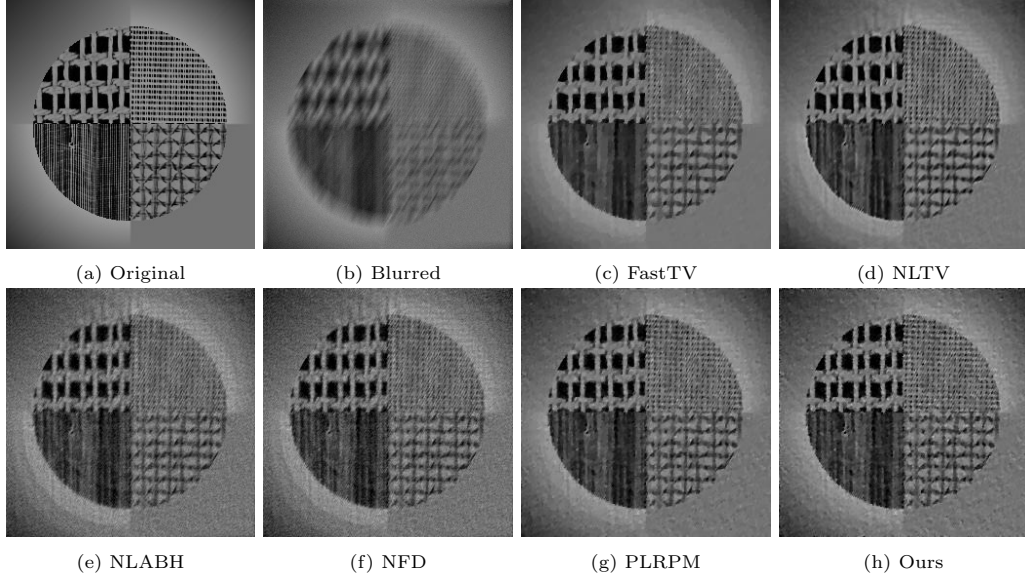


Figure 9: Recovery results for the hybrid image with motion blur and corrupted by the noise of standard deviation $\sigma = 3$. (a) original image. (b) noisy blurred image, PSNR=18.07. (c)-(h) recovered images.

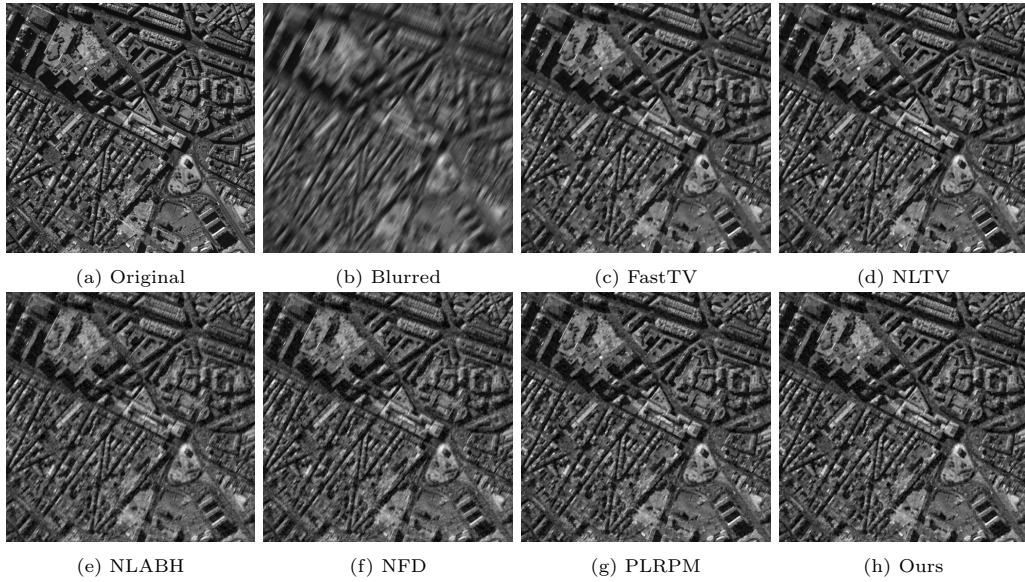


Figure 10: Recovery results for the satellite1 image with motion blur and corrupted by the noise of standard deviation $\sigma = 3$. (a) original image. (b) noisy blurred image, PSNR=18.64. (c)-(h) recovered images.

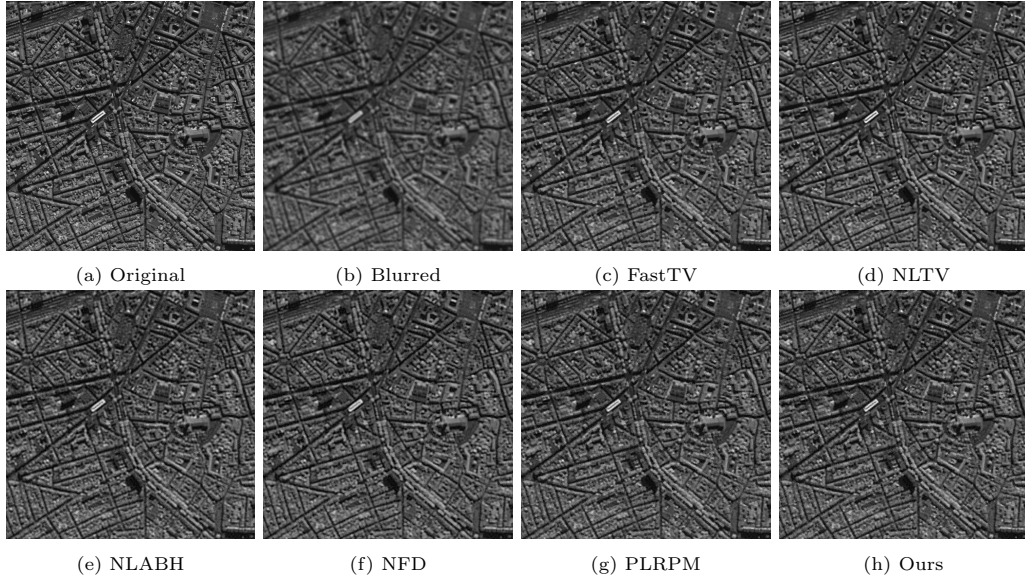


Figure 11: Recovery results for the satellite2 image with disk blur and corrupted by the noise of standard deviation $\sigma = 3$. (a) original image. (b) noisy blurred image, PSNR=21.68. (c)-(h) recovered images.

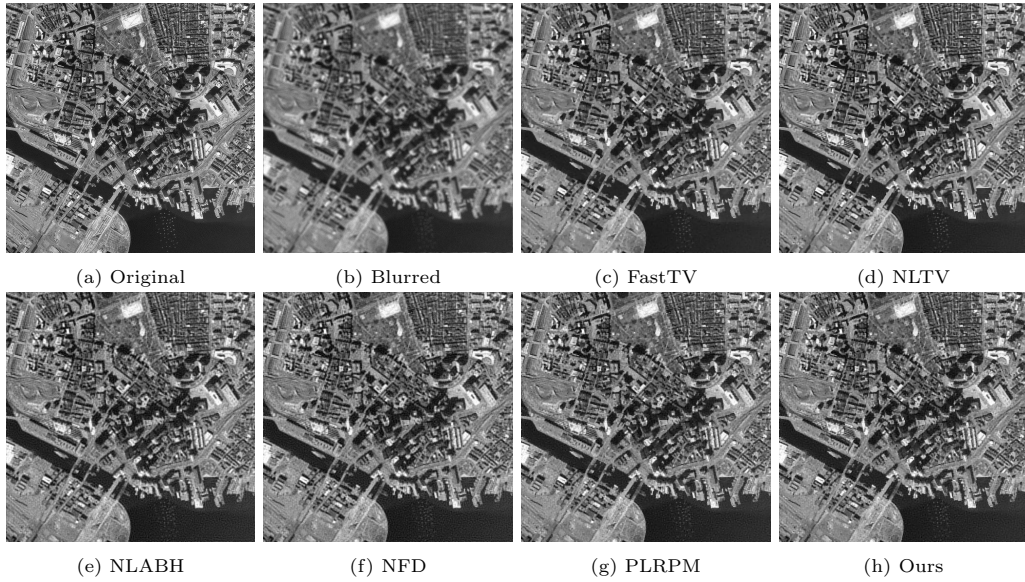


Figure 12: Recovery results for the satellite3 image with average blur and corrupted by the noise of standard deviation $\sigma = 3$. (a) original image. (b) noisy blurred image, PSNR=19.20. (c)-(h) recovered images.

and texture2 are shown in Figs. 7 and 8. Texture1 and texture2 images are blurred by disk kernel and average kernel, respectively. For these two experiments, we select $\lambda = 45$ in the proposed model. We find that in Figs. 7c and 8c, there is minimal noise present, but the visual quality is over-smooth, with an evident loss of texture information. On the other hand, in Figs. 7e, 7f, 8e and 8f, texture details are better preserved, however, there is an increase in the noise level of the images. Compared to Figs. 7d, 8d, 7g and 8g, the restoration results of the proposed model exhibit slightly higher noise levels but retain more texture information, resulting in a better visual quality, see Figs. 7h and 8h. For a detailed comparison, we also present zoomed-in views of a selected region from the texture1 image in Fig. 13a. The corresponding restoration results for this region are shown in Fig. 14.

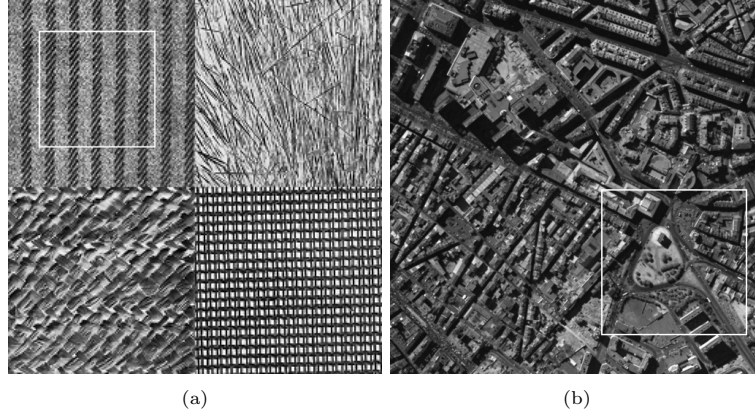


Figure 13: The original texture1 image and satellite1 image, the marked squares are marked for zooming.

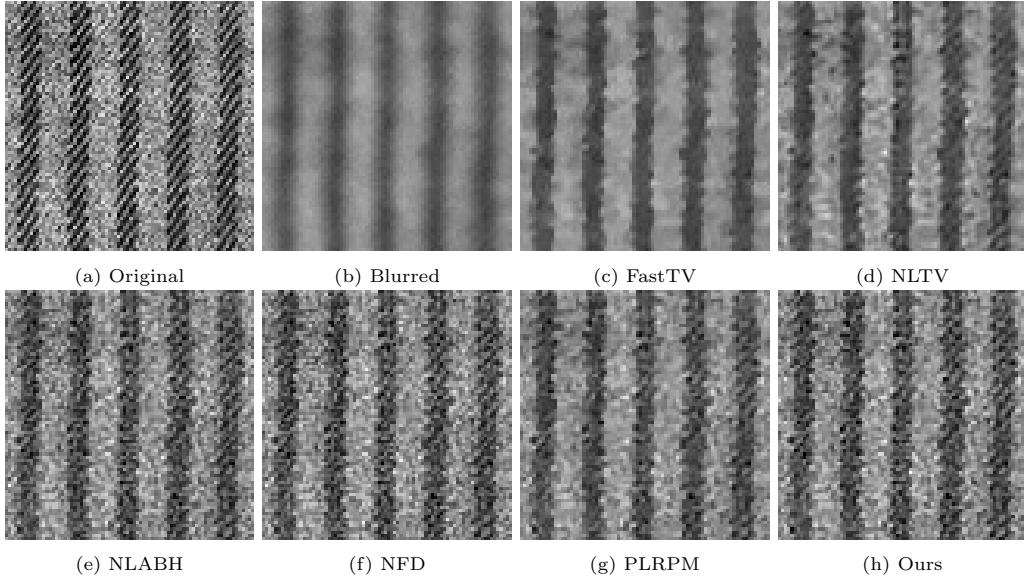


Figure 14: Zoomed-in images corresponding to the results shown in Fig. 7.

For the restoration results of the hybrid image, some new phenomena emerge, as illustrated in Fig. 9. The central area of the hybrid image is rich in texture, while the surrounding area is smooth, as shown in Fig. 9a. The hybrid image is blurred by a motion kernel, posing a challenge for all models, see Fig. 9b. For this experiment, we select $\lambda = 15$ in the proposed model. It is observed from Fig. 9c that the restoration result of FastTV contains fewer noise and artifacts in smooth areas, but it fails to preserve texture information.

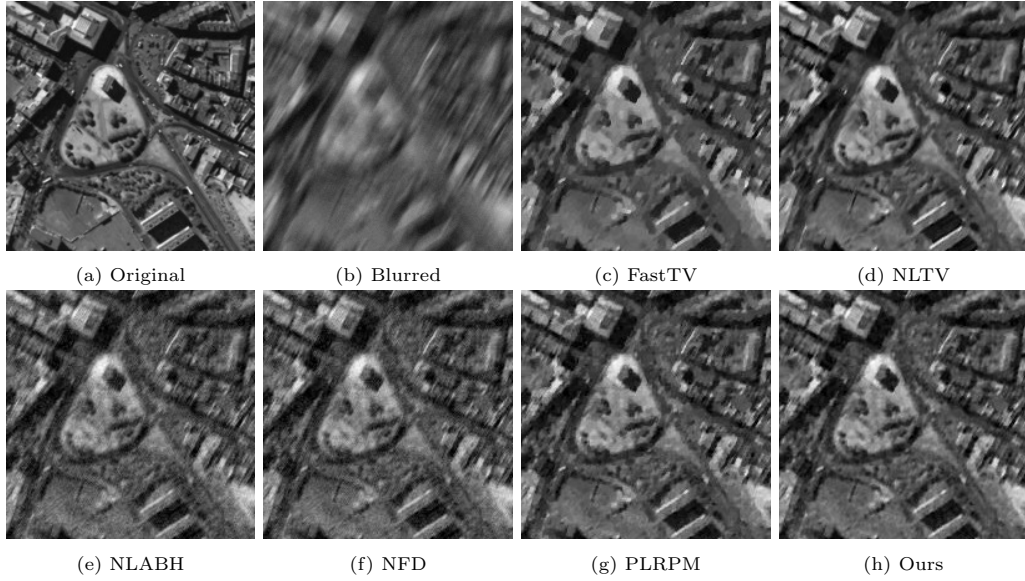


Figure 15: Zoomed-in images corresponding to the results shown in Fig. 10.

NLABH and NFD noticeably amplify noise in smooth regions and produce obvious artifacts, as seen in Figs. 9e and 9f. In the restoration results of the proposed model, noise in smooth areas is slightly more pronounced compared to NLTv and PLRPM, but texture preservation is better than PLRPM, and there are no artifacts in smooth regions as seen in the restoration results of NLTv, see Figs. 9d, 9g, and 9h.

Finally, the restoration results for three satellite images are shown in Figs. 10-12. The three satellite images are respectively blurred by motion kernel, disk kernel, and average kernel, as shown in Figs. 10b, 11b, and 12b. We select $\lambda = 15, 15, 10$ in the proposed model respectively for these three experiments. Similar to the previous experiments, the restoration results of FastTV and NLTv are relatively smooth, and the noise levels in the restoration results of NLABH and NFD are increased. Overall, the methods with better visual restoration results are NLTv, PLRPM, and the proposed method. Our method slightly reduces visual quality on satellite3 due to increased noise in smooth regions, but performs best on satellite1 and satellite2, as shown in Figs. 10h, 11h, and 12h. Fig. 15 shows the zoomed-in restoration results corresponding to the selected region of the satellite1 image in Fig. 13b.

6. Final remarks

The local well-posedness of the proposed model and the regularity of local solutions have been investigated. We hope that our work helps fill a gap in the theoretical analysis of similar image processing problems and may offer useful insight for future studies. Establishing global well-posedness conditions and the characterization of the steady-state limit for the general case are open and challenging problems that need further study. We point out that the considered model does not possess a variational structure, and whether it can be explained from an energy point of view remains to be studied. It should also be emphasized that the theoretical analysis in this paper does not cover the case $\inf_{x \in \Omega} f(x) = 0$, which introduces extra degeneracy and prevents the use of maximal regularity theory. Addressing this case may require brand-new ideas and techniques. Finally, numerical experiments have verified the effectiveness of the proposed model, while the design of fast algorithms that allow larger time steps represents another interesting direction for future work.

References

- [1] H. Amann, Dynamic theory of quasilinear parabolic equations. II. Reaction-diffusion systems, *Differ. Integr. Equations* 3 (1990) 13–75. <https://doi.org/10.57262/die/1371586185>.
- [2] H. Amann, *Nonhomogeneous Linear and Quasilinear Elliptic and Parabolic Boundary Value Problems*, Vieweg+Teubner Verlag, Wiesbaden, 1993, pp. 9–126.
- [3] H. Amann, *Linear and Quasilinear Parabolic Problems*, Birkhäuser, Basel-Boston-Berlin, 1995.
- [4] H. Amann, Maximal regularity for nonautonomous evolution equations, *Adv. Nonlinear Stud.* 4 (2004) 417–430. <https://doi.org/10.1515/ans-2004-0404>.
- [5] H. Amann, Quasilinear parabolic problems via maximal regularity, *Adv. Differ. Equations* 10 (2005) 1081–1110. <https://doi.org/10.57262/ade/1355867805>.
- [6] H. Amann, M. Hieber, G. Simonett, Bounded H_∞ -calculus for elliptic operators, *Differ. Integr. Equations* 7 (1994) 613–653. <https://doi.org/10.57262/die/1370267697>.
- [7] G. Aubert, L. Vese, A variational method in image recovery, *SIAM J. Numer. Anal.* 34 (1997) 1948–1979. <https://doi.org/10.1137/S003614299529230X>.
- [8] J. Bai, X. C. Feng, Fractional-order anisotropic diffusion for image denoising, *IEEE Trans. Image Process.* 16 (2007) 2492–2502. <https://doi.org/10.1109/TIP.2007.904971>.
- [9] T. Barbu, *Novel Diffusion-Based Models for Image Restoration and Interpolation*, Springer, Cham, 2019. <https://doi.org/10.1007/978-3-319-93006>.
- [10] G. I. Barenblatt, V. M. Entov, V. M. Ryzhik, *Theory of fluid flows through natural rocks*, volume 395, Springer, Dordrecht, 1990.
- [11] A. L. Bertozzi, J. B. Greer, Low-curvature image simplifiers: Global regularity of smooth solutions and Laplacian limiting schemes, *Commun. Pure Appl. Math.* 57 (2004) 764–790. <https://doi.org/10.1002/cpa.20019>.
- [12] J. Boussinesq, Recherches théoriques sur l’écoulement des nappes d’eau infiltrées dans le sol et sur le débit des sources, *J. Math. Pures Appl.* 10 (1904) 5–78.
- [13] K. Bredies, K. Kunisch, T. Pock, Total generalized variation, *SIAM J. Imag. Sci.* 3 (2010) 492–526. <https://doi.org/10.1137/090769521>.
- [14] J.-F. Cai, B. Dong, S. Osher, Z. Shen, Image restoration: Total variation, wavelet frames, and beyond, *J. Amer. Math. Soc.* 25 (2012) 1033–1089. <https://doi.org/10.1090/S0894-0347-2012-00740-1>.
- [15] F. Catté, P. L. Lions, J. M. Morel, T. Coll, Image selective smoothing and edge detection by nonlinear diffusion, *SIAM J. Numer. Anal.* 29 (1992) 182–193. <https://doi.org/10.1137/0729012>.
- [16] R. H. Chan, A. Lanza, S. Morigi, F. Sgallari, An adaptive strategy for the restoration of textured images using fractional order regularization, *Numer. Math. Theory Methods Appl.* 6 (2013) 276–296. <https://doi.org/10.4208/nmtma.2013.mssvm15>.
- [17] T. F. Chan, J. Shen, *Image Processing and Analysis: Variational, PDE, Wavelet, and Stochastic Methods*, SIAM, Philadelphia, 2005. <https://doi.org/10.1137/1.9780898717877>.
- [18] R. Chiappinelli, R. Nugari, The Nemitskii operator in hölder spaces: some necessary and sufficient conditions, *J. London Math. Soc.* 51 (1995) 365–372. <https://doi.org/10.1112/jlms/51.2.365>.
- [19] K. J. Engel, R. Nagel, S. Brendle, *One-parameter semigroups for linear evolution equations*, Springer, New York, 2000.
- [20] A. Friedman, *Partial Differential Equations of Parabolic Type*, R.E. Krieger Publishing Company, Malabar, 1983.
- [21] N. Galatsanos, A. Katsaggelos, Methods for choosing the regularization parameter and estimating the noise variance in image restoration and their relation, *IEEE Trans. Image Process.* 1 (1992) 322–336. <https://doi.org/10.1109/83.148606>.
- [22] G. Gilboa, S. Osher, Nonlocal linear image regularization and supervised segmentation, *Multiscale Model. Sim.* 6 (2007) 595–630. <https://doi.org/10.1137/060669358>.
- [23] G. Gilboa, S. Osher, Nonlocal operators with applications to image processing, *Multiscale Model. Sim.* 7 (2009) 1005–1028. <https://doi.org/10.1137/070698592>.
- [24] P. Guidotti, A new nonlocal nonlinear diffusion of image processing, *J. Differential Equations* 246 (2009) 4731–4742. <https://doi.org/10.1016/j.jde.2009.03.017>.
- [25] P. Guidotti, A new well-posed nonlinear nonlocal diffusion, *Nonlinear Anal.* 72 (2010) 4625–4637. <https://doi.org/10.1016/j.na.2010.02.040>.
- [26] P. Guidotti, A backward-forward regularization of the Perona–Malik equation, *J. Differential Equations* 252 (2012) 3226–3244. <https://doi.org/10.1016/j.jde.2011.10.022>.
- [27] P. Guidotti, Anisotropic diffusions of image processing from Perona–Malik on, in: *Variational methods for evolving objects*, volume 67 of *Adv. Stud. Pure Math.*, Math. Soc. Japan, Tokyo, 2015, pp. 131–156. <https://doi.org/10.2969/aspm/06710131>.
- [28] P. Guidotti, Y. Kim, J. Lambers, Image restoration with a new class of forward-backward-forward diffusion equations of Perona–Malik type with applications to satellite image enhancement, *SIAM J. Imag. Sci.* 6 (2013) 1416–1444. <https://doi.org/10.1137/120882895>.
- [29] P. Guidotti, K. Longo, Well-posedness for a class of fourth order diffusions for image processing, *Nonlinear Differ. Equations Appl.* 18 (2011) 407–425. <https://doi.org/10.1007/s00030-011-0101-x>.
- [30] Z. Guo, W. Yao, J. Sun, B. Wu, Nonlinear fractional diffusion model for deblurring images with textures, *Inverse Probl. Imaging* 13 (2019) 1161–1188. <https://doi.org/10.3934/ipi.2019052>.
- [31] M. Hieber, J. Prüss, Heat kernels and maximal L_p - L_q estimates for parabolic evolution equations, *Commun. Partial Differ. Equations* 22 (1997) 1647–1669. <https://doi.org/10.1080/03605309708821314>.

- [32] Y. Huang, M. K. Ng, Y. W. Wen, A fast total variation minimization method for image restoration, *Multiscale Model. Sim.* 7 (2008) 774–795. <https://doi.org/10.1137/070703533>.
- [33] S. Kindermann, S. Osher, P. W. Jones, Deblurring and denoising of images by nonlocal functionals, *Multiscale Model. Sim.* 4 (2005) 1091–1115. <https://doi.org/10.1137/050622249>.
- [34] P. C. Kunstmann, L. Weis, Maximal L_p -regularity for parabolic equations, *Fourier Multiplier Theorems and H^∞ -functional Calculus*, Springer Berlin Heidelberg, Berlin, Heidelberg, 2004, pp. 65–311.
- [35] A. Langer, Automated parameter selection for total variation minimization in image restoration, *J. Math. Imaging Vision* 57 (2017) 239–268. <https://doi.org/10.1007/s10851-016-0676-2>.
- [36] G. Leoni, *A first course in fractional Sobolev spaces*, American Mathematical Society, Providence, RI, 2023. <https://doi.org/10.1090/gsm/229>.
- [37] A. Lunardi, *Analytic semigroups and optimal regularity in parabolic problems*, Birkhäuser, Basel, 1995.
- [38] M. Lysaker, A. Lundervold, X.-C. Tai, Noise removal using fourth-order partial differential equation with applications to medical magnetic resonance images in space and time, *IEEE Trans. Image Process.* 12 (2003) 1579–1590. <https://doi.org/10.1109/TIP.2003.819229>.
- [39] S. Majee, R. K. Ray, A. K. Majee, A gray level indicator-based regularized telegraph diffusion model: Application to image despeckling, *SIAM J. Imag. Sci.* 13 (2020) 844–870. <https://doi.org/10.1137/19M1283033>.
- [40] H. Mehrer, *Diffusion in Solids: Fundamentals, Methods, Materials, Diffusion-Controlled Processes*, Springer, Berlin, Heidelberg, 2007. <https://doi.org/10.1007/978-3-540-71488-0>.
- [41] S. Morigi, L. Reichel, F. Sgallari, A. Shyshkov, Cascadic multiresolution methods for image deblurring, *SIAM J. Imag. Sci.* 1 (2008) 51–74. <https://doi.org/10.1137/070694065>.
- [42] M. Muskat, The flow of fluids through porous media, *J. Appl. Phys.* 8 (1937) 274–282. <https://doi.org/10.1063/1.1710292>.
- [43] P. Perona, J. Malik, Scale-space and edge detection using anisotropic diffusion, *IEEE Trans. Pattern Anal. Mach. Intell.* 12 (1990) 629–639. <https://doi.org/10.1109/34.56205>.
- [44] C. Poynton, *Digital video and HD: Algorithms and Interfaces*, second edition ed., Morgan Kaufmann, Boston, 2012.
- [45] J. Prüss, G. Simonett, R. Zacher, On convergence of solutions to equilibria for quasilinear parabolic problems, *J. Differential Equations* 246 (2009) 3902–3931. <https://doi.org/10.1016/j.jde.2008.10.034>.
- [46] M. R. Roussel, *Nonlinear Dynamics*, Morgan & Claypool Publishers, San Rafael, CA, 2019. <https://doi.org/10.1088/2053-2571/ab0281>.
- [47] L. I. Rudin, S. Osher, Total variation based image restoration with free local constraints, in: *Proceedings of 1st International Conference on Image Processing*, volume 1, 1994, pp. 31–35.
- [48] L. I. Rudin, S. Osher, E. Fatemi, Nonlinear total variation based noise removal algorithms, *Physica D* 60 (1992) 259–268. [https://doi.org/10.1016/0167-2789\(92\)90242-F](https://doi.org/10.1016/0167-2789(92)90242-F).
- [49] V. S. Rychkov, On restrictions and extensions of the Besov and Triebel–Lizorkin spaces with respect to Lipschitz domains, *J. London Math. Soc.* 60 (1999) 237–257. <https://doi.org/10.1112/S0024610799007723>.
- [50] Y. Sawano, *Theory of Besov Spaces*, Springer, Singapore, 2018. <https://doi.org/10.1007/978-981-13-0836-9>.
- [51] R. Schumer, D. A. Benson, M. M. Meerschaert, S. W. Wheatcraft, Eulerian derivation of the fractional advection-dispersion equation, *J. Contam. Hydrol.* 48 (2001) 69–88. [https://doi.org/10.1016/S0169-7722\(00\)00170-4](https://doi.org/10.1016/S0169-7722(00)00170-4).
- [52] X. Shan, J. Sun, Z. Guo, Multiplicative noise removal based on the smooth diffusion equation, *J. Math. Imaging Vision* 61 (2019) 763–779. <https://doi.org/10.1007/s10851-018-00870-z>.
- [53] X. Shan, J. Sun, Z. Guo, W. Yao, Z. Zhou, Fractional-order diffusion model for multiplicative noise removal in texture-rich images and its fast explicit diffusion solving, *BIT Numer. Math.* 62 (2022) 1319–1354. <https://doi.org/10.1007/s10543-022-00913-3>.
- [54] K. Shi, Image denoising by nonlinear nonlocal diffusion equations, *J. Comput. Appl. Math.* 395 (2021) 113605. <https://doi.org/10.1016/j.cam.2021.113605>.
- [55] M. Šilhavý, Fractional vector analysis based on invariance requirements (critique of coordinate approaches), *Continuum Mech. Thermodyn.* 32 (2020) 207–228. <https://doi.org/10.1007/s00161-019-00797-9>.
- [56] V. A. Solonnikov, *Boundary value problems of mathematical physics. III*, Amer. Math. Soc, Providence, 1967.
- [57] J. C. Strikwerda, *Finite Difference Schemes and Partial Differential Equations*, second edition ed., SIAM, Philadelphia, 2004. <https://doi.org/10.1137/1.9780898717938>.
- [58] H. Takeda, S. Farsiu, P. Milanfar, Deblurring using regularized locally adaptive kernel regression, *IEEE Trans. Image Process.* 17 (2008) 550–563. <https://doi.org/10.1109/TIP.2007.918028>.
- [59] A. N. Tikhonov, V. Y. Arsenin, *Solutions of Ill-Posed Problems*, John Wiley & Sons, New York, 1977.
- [60] H. Triebel, *Interpolation Theory, Function Spaces, Differential Operators*, North-Holland Publishing Co., Amsterdam-New York, 1978.
- [61] J. L. Vazquez, *The Porous Medium Equation: Mathematical Theory*, Oxford University Press, New York, 2006.
- [62] V. Volpert, *Reaction-diffusion Processes, Models and Applications*, Springer, Basel, 2014. <https://doi.org/10.1007/978-3-0348-0813-2>.
- [63] J. Weickert, A review of nonlinear diffusion filtering, in: B. ter Haar Romeny, L. Florack, J. Koenderink, M. Viergever (Eds.), *Scale-Space Theory in Computer Vision*, Springer Berlin Heidelberg, Berlin, Heidelberg, 1997, pp. 1–28.
- [64] J. Weickert, *Anisotropic Diffusion in Image Processing*, ECMI, B. G. Teubner Verlag, Stuttgart, Germany, 1998. <https://doi.org/10.1109/83.661190>.
- [65] J. Weickert, B. Benhamouda, A semidiscrete nonlinear scale-space theory and its relation to the Perona–Malik paradox, in: F. Solina, W. G. Kropatsch, R. Klette, R. Bajcsy (Eds.), *Advances in Computer Vision*, Springer, Vienna, 1997, pp. 1–10.

- [66] J. Weickert, S. Grewenig, C. Schroers, A. Bruhn, Cyclic schemes for PDE-based image analysis, *Int. J. Comput. Vis.* 118 (2016) 275–299. <https://doi.org/10.1007/s11263-015-0874-1>.
- [67] M. Welk, D. Theis, T. Brox, J. Weickert, PDE-based deconvolution with forward-backward diffusivities and diffusion tensors, in: R. Kimmel, N. A. Sochen, J. Weickert (Eds.), *Scale Space and PDE Methods in Computer Vision*, Springer Berlin Heidelberg, Berlin, Heidelberg, 2005, pp. 585–597.
- [68] Y. Wen, J. Sun, Z. Guo, A new anisotropic fourth-order diffusion equation model based on image features for image denoising, *Inverse Probl. Imaging* 16 (2022) 895–924. <https://doi.org/10.3934/ipi.2022004>.
- [69] Y. Wen, L. A. Vese, K. Shi, Z. Guo, J. Sun, Nonlocal adaptive biharmonic regularizer for image restoration, *J. Math. Imaging Vision* 65 (2023) 453–471. <https://doi.org/10.1007/s10851-022-01129-4>.
- [70] W. Yao, Z. Guo, J. Sun, B. Wu, H. Gao, Multiplicative noise removal for texture images based on adaptive anisotropic fractional diffusion equations, *SIAM J. Imag. Sci.* 12 (2019) 839–873. <https://doi.org/10.1137/18M1187192>.
- [71] X. Yin, S. Zhou, M. A. Siddique, Fractional nonlinear anisotropic diffusion with p -Laplace variation method for image restoration, *Multimedia Tools Appl.* 75 (2016) 4505–4526. <https://doi.org/10.1007/s11042-015-2488-6>.
- [72] Y. L. You, M. Kaveh, Fourth-order partial differential equations for noise removal, *IEEE Trans. Image Process.* 9 (2000) 1723–1730. <https://doi.org/10.1109/83.869184>.
- [73] Y. B. Zel'Dovich, Y. P. Raizer, *Physics of shock waves and high-temperature hydrodynamic phenomena*, Academic Press, NY & London, 2002.
- [74] J. Zhang, K. Chen, A total fractional-order variation model for image restoration with nonhomogeneous boundary conditions and its numerical solution, *SIAM J. Imag. Sci.* 8 (2015) 2487–2518. <https://doi.org/10.1137/14097121X>.
- [75] X. Zhang, M. Burger, X. Bresson, S. Osher, Bregmanized nonlocal regularization for deconvolution and sparse reconstruction, *SIAM J. Imag. Sci.* 3 (2010) 253–276. <https://doi.org/10.1137/090746379>.
- [76] X. Zhao, K. Huang, X. Wang, M. Shi, X. Zhu, Q. Gao, Z. Yu, Reaction–diffusion equation based image restoration, *Appl. Math. Comput.* 338 (2018) 588–606. <https://doi.org/10.1016/j.amc.2018.06.054>.
- [77] Z. Zhou, Z. Guo, G. Dong, J. Sun, D. Zhang, B. Wu, A doubly degenerate diffusion model based on the gray level indicator for multiplicative noise removal, *IEEE Trans. Image Process.* 24 (2015) 249–260. <https://doi.org/10.1109/TIP.2014.2376185>.
- [78] Z. Zhou, Z. Guo, D. Zhang, B. Wu, A nonlinear diffusion equation-based model for ultrasound speckle noise removal, *J. Nonlinear Sci.* 28 (2018) 443–470. <https://doi.org/10.1007/s00332-017-9414-1>.